10-1-2020

Comparisons of upper air ozone at a coastal and urban site and the impacts of non-controllable ozone sources

Chloe Gore
San Jose State University

Sen Chiao
San Jose State University, sen.chiao@sjsu.edu

Recommended Citation

Chloe Gore and Sen Chiao. "Comparisons of upper air ozone at a coastal and urban site and the impacts of non-controllable ozone sources" *Atmospheric Environment: X* (2020). https://doi.org/10.1016/j.aeaoa.2020.100085

ATMOSPHERIC ENVIRONMENT: X 7 (2020) 100085

Contents lists available at ScienceDirect

Atmospheric Environment: X

journal homepage: http://www.journals.elsevier.com/atmospheric-environment-x

Comparisons of upper air ozone at a coastal and urban site and the impacts of non-controllable ozone sources

Chloe Gore, Sen Chiao *

Center for Applied Atmospheric Research and Education, San Jose State University, USA

ARTICLE INFO

Keywords:
Upper air ozone
Urban
Surface emission
Planetary boundary layer

ABSTRACT

This study quantified the impact of non-controllable and urban emission sources on the enhancement of ozone (O_3) in the troposphere. These enhancements were investigated using data from simultaneous ozonesonde launches at Half Moon Bay (HMB), CA and San Jose (SJ), CA on eleven dates in July and August 2018. The urban O_3 enhancement in the SJ vertical profile was derived by subtracting out HMB, which represents baseline O_3, from the urban SJ profile. Within the planetary boundary layer (PBL), urban emissions had a large impact on SJ, as SJ O_3 was 20–30 ppb higher than HMB for all dates. Above the PBL, most enhancement profiles remained close to zero, indicating little differences aloft between HMB and SJ. The two sites had strong correlation coefficients (CCs), highlighting the influence of baseline O_3 on SJ. A major axis regression for all vertical levels between SJ and HMB revealed a slope of 1.00 SJ ppb/HMB ppb and intercept of 0.004 ppb. The percent contribution of mixing layer (ML) O_3 to tropospheric O_3 and tropospheric O_3 to total column O_3 demonstrates the predominant influence of baseline O_3 on the O_3 profile, even over a polluted urban region. The contribution of ML O_3 was low for all dates, between 2 and 6%, whereas the tropospheric contribution was 11–18%. These findings emphasize the importance of baseline O_3 in regions with reduced vertical mixing; polluted urban air near the surface has minimal impacts on O_3 concentrations above the PBL.

1. Introduction

Ozone (O_3) is a secondary air pollutant formed primarily through the photochemical oxidation of carbon monoxide (CO) and volatile organic compounds (VOC) in the presence of nitrogen oxides (NO_x) (Fiore et al., 2002; Wu et al., 2008; Jaffe et al., 2018). Prior studies (e.g., Smith et al., 2009; Ostro et al., 2012; Bell et al., 2006; Anenberg et al., 2010; Turner et al., 2016; Berman et al., 2012; Ellingsen et al., 2008; Rai and Agrawai, 2012; Avnery et al., 2011a,b) have confirmed that in the troposphere, O_3 is harmful to human health and vegetation. In 2015, the Environmental Protection Agency (EPA) lowered the National Ambient Air Quality Standard (NAAQS) for ozone from 75 ppb to 70 ppb (Environmental Protection Agency, 2015). By definition, the NAAQS is met when the three-year average of the annual fourth-highest daily maximum 8-h ozone concentration is less than or equal to 70 ppb (U.S. Environmental Protection Agency, 1998; 2105). In order to protect public health and meet the NAAQS for ozone, it is important to monitor O_3 trends and design emission control strategies to reduce O_3 concentrations and O_3 precursor species.

Studies observing these tropospheric O_3 trends have found a decrease in the overall variability and range (difference between days of low and high O_3 mixing ratios) of surface O_3 concentrations in numerous regions across the U.S. (Lefohn et al., 2010; Cooper et al., 2012; Simon et al., 2015). In the western U.S., observed background O_3 trends are shown to be increasing up to the mid 2000s (Jaffe et al., 2003; Jaffe and Ray, 2007; Cooper et al., 2010) and have since begun to decrease (Parrish et al., 2017). This decrease should help regions in the western U.S. maintain the NAAQS standard, which has been a challenge in the past due to the influence of baseline O_3. Baseline O_3 is defined by the Task Force on Hemispheric Transport of Air Pollution (HTAP) as an O_3 concentration observed at a site uninfluenced by local anthropogenic activities (Cooper et al., 2011; Task Force on Hemispheric Transport of Air Pollution, 2010; Cooper et al., 2015).

Western coastal sites are largely impacted by synoptic transport of air masses across the Pacific. These air masses can transport high O_3 concentrations from the Asian continent, increasing baseline O_3 concentrations and creating challenges for improving local air quality (Oltmans et al., 2008; Cooper et al., 2010; Lin et al., 2017; Hudman

* Corresponding author. Dept Meteorology and Climate Science, San Jose State University, USA.
E-mail address: sen.chiao@sjsu.edu (S. Chiao).

https://doi.org/10.1016/j.aeaoa.2020.100085
Received 27 August 2019; Received in revised form 21 June 2020; Accepted 6 July 2020
Available online 10 July 2020

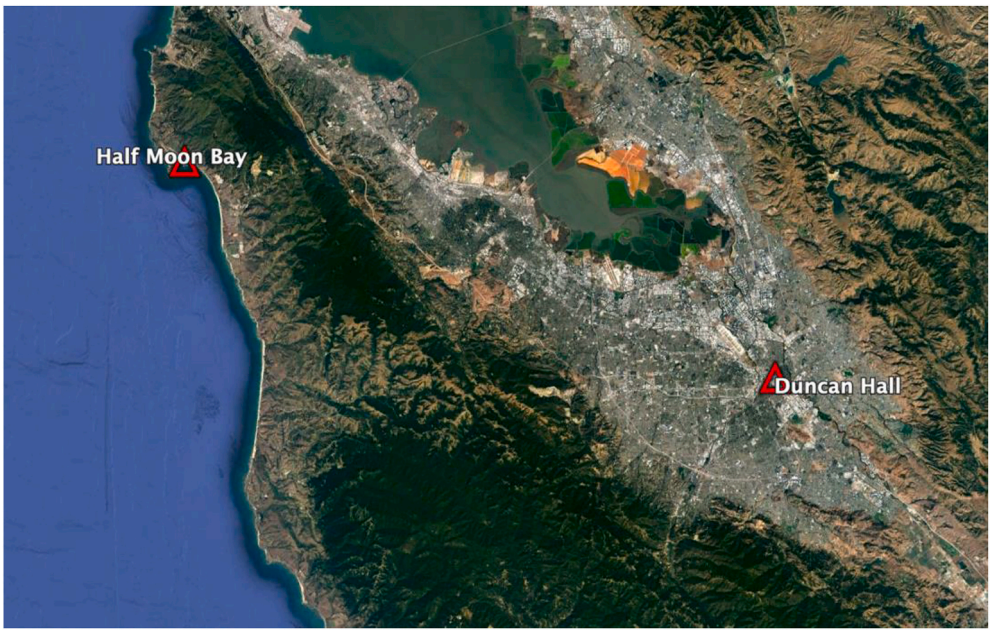

Fig. 1. Location of ozonesonde launches (red triangle). Duncan Hall represents the San Jose, CA site, as it is located next to downtown. (For interpretation of the references to colour in this figure legend, the reader is referred to the Web version of this article.)

et al., 2004; Ryoo et al., 2017). Additionally, Ryoo et al., (2017) examined a high O_3 event off the central California coast on May 30, 2012, and determined that Asian transport had a large impact on the air masses reaching the western U.S. Forward model trajectories also indicated that this transported high-O_3 air could affect inland surface concentrations. Parrish et al., (2014) concluded that the lifetime of tropospheric O_3 is within the temporal scale for transport between continents. They further noted that, aside from urban regions, this baseline O_3 inflow is the controlling source of observed O_3 concentrations.

Elevated O_3 levels are also influenced by stratospheric intrusions (SI) (e.g., Langford et al., 2017; Langford et al., 2015; Lin et al., 2012; Langford et al., 2018; Clark and Chiao, 2019). SIs typically result from tropopause folding, which entrains high O_3 stratospheric air into the free troposphere (Langford et al., 2018). Lin et al. (2015a) examined how climate variability impacts SIs and found that after strong La Nina winters, there is an increase in late spring SIs in the Western U.S. due to the northward shift of the polar jet stream into the Pacific Northwest. Zhang et al., (2014) determined that lightning increases surface O_3 mean levels and that SIs result in the highest O_3 concentrations in the Intermountain West. They also examined the relationship between O_3 levels and wildfires, however did not reach a definitive conclusion. California anthropogenic emissions were determined to increase surface O_3 concentrations downwind, as well.

The processes impacting O_3 are spatially large scale, as demonstrated by Logan et al., (2012), who determined that a similar temporal variability of tropospheric O_3 is present for the 500–1000 km scale. For example, Baylon et al., (2016) examined the impact of baseline O_3 measured at Mount Bachelor Observatory (MBO) on surface O_3 at various sites in the Western U.S. and found that, under conducive meteorological conditions, the length of the surface station O_3 correlation is 850 km. Similarly, Wigder et al., (2013) assessed the transport of tropospheric O_3 from MBO to Boise and marine boundary layer O_3 from Cheeka Peak, WA to Enumclaw, WA and determined that, when the air mass influences Boise's MDA8 O_3, MBO explained 40% of Boise's MDA8 variation and Cheeka Peak explains 69% of Enumclaw MDA8 variations.

O_3 concentrations are also influenced by various meteorological parameters. Solar radiation drives photochemical reactions of O_3 precursor species (e.g., NO_x), therefore ample sunlight is favorable for high O_3 production (Pudasainee et al., 2006). O_3 exhibits a diurnal pattern, with high concentrations during the daytime and low concentrations at night, while the precursors (e.g. NO_x) have an opposite pattern (Tu et al., 2007). Seaman and Michelson (2000) identified synoptic conditions favorable for O_3 production, including high temperatures, light winds, and minimal cloud cover. This is consistent with observations that indicate stable conditions are ideal for high O_3 and poor air quality events. Knowledge of these characteristics is important for understanding O_3 formation and the causes of high O_3 episodes.

O_3 concentrations are also influenced by precursor emissions (Wigder et al., 2013). Increases in NO_x and VOCs have been shown to lead to O_3 increases (Wei et al., 2014; John et al., 1998; David and Nair, 2011; Pusede and Cohen, 2012; Gorai et al., 2015; Grewe et al., 2012). Carbon monoxide (CO) is a known precursor to O_3; under photochemical conditions, CO and O_3 have a positively correlated relationship (Chin et al., 1994; Fishman and Seiler, 1983; Gilge et al., 2010; Macdonald et al., 2011). Methane (CH_4) can also act as a precursor to O_3, however due to the long lifetime of CH_4, these studies are primarily modeling analyses (Shindell et al., 2005; Dentener et al., 2005; West et al., 2006; Fiore et al., 2002). O_3 photochemical formation is not a linear process. Increases in the precursor NO_x do not consistently lead to O_3 increases and can sometimes cause decreases. This response depends on existing ambient conditions and VOC/NO_x concentrations (e.g., Konovalov, 2002; Xiao et al., 2010). Consequently, the nonlinearity of O_3 formation creates challenges for source attribution of O_3 concentrations.

O_3 precursors are prevalent in urban regions as a result of the dense population, which leads to increased automobile activity, higher energy demands, etc. (Marcotullio et al., 2013; Dodman, 2011). Urban locations in the western U.S. have additional challenges for reducing O_3 concentrations due to the combination of O_3 precursor emissions and high concentrations of baseline O_3. For example, Cooper et al. (2012) observed decreases in rural O_3 concentrations across the eastern United States in spring and summer months from 1990 to 2010, while the western sites had more significant increasing than decreasing trends. Additionally, Lin et al. (2015b) observed springtime increasing O_3 trends in western North America over the last decade and increasing background trends.

Although O_3 studies have been conducted for northern and southern California (Goldstein et al., 2004; Croes and Fujita, 2003; Cooper et al.,

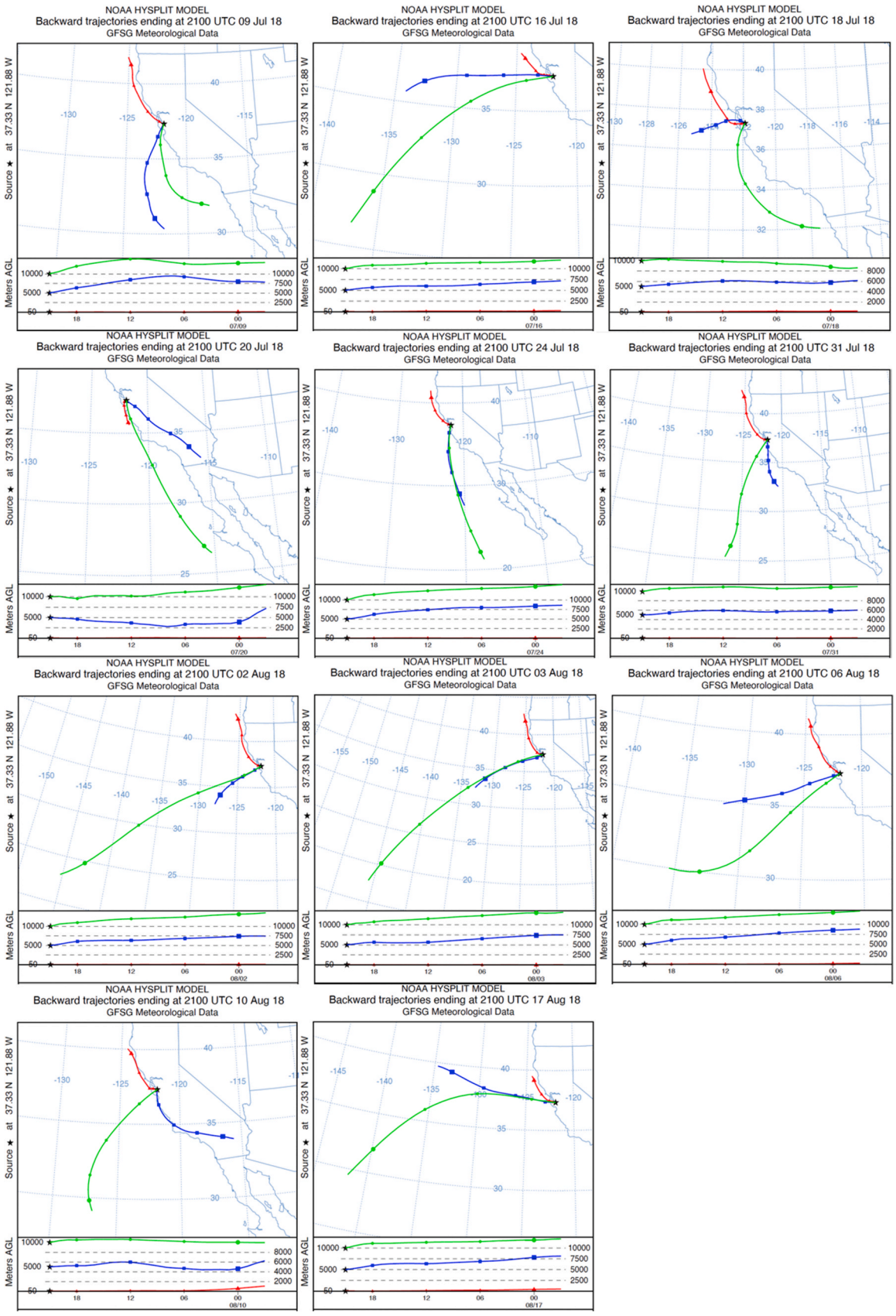

Fig. 2. NOAA HYSPLIT backwards trajectories from SJ (Duncan Hall) for each launch date. The red line is 0 km, blue line is 5 km, and green line is 10 km. (For interpretation of the references to colour in this figure legend, the reader is referred to the Web version of this article.)

Table 1
Correlations between HMB and SJ profiles.

Date	Correlation Coefficient	P-Value
July 9, 2018	0.93	0.0
July 16, 2018	0.83	0.0
July 18, 2018	0.88	0.0
July 20, 2018	0.84	0.0
July 24, 2018	0.91	0.0
July 31, 2018	0.72	0.0
August 2, 2018	0.92	0.0
August 3, 2018	0.87	0.0
August 6, 2018	0.68	0.0
August 10, 2018	0.85	0.0
August 17, 2018	0.92	0.0
All dates	0.79	0.0

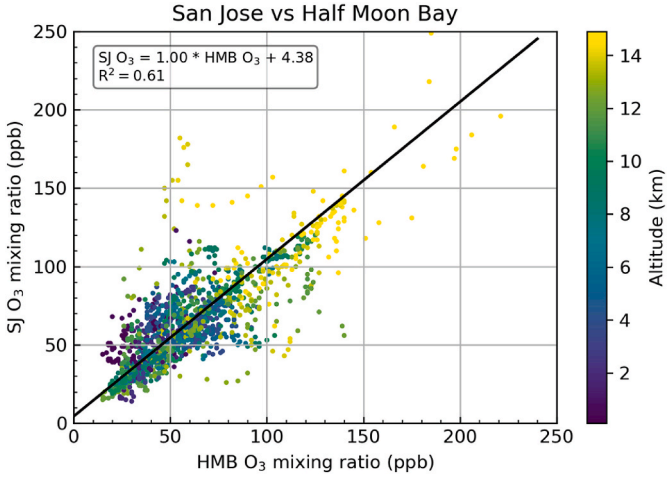

Fig. 3. Scatter plot of San Jose O_3 mixing ratios (ppb) and Half Moon Bay O_3 mixing ratios (ppb) with a major axis regression line in black. Slope = 1.00 SJ ppb/HMB ppb and intercept = 4.38 ppb.

2011; Yates et al., 2013), to further advance our understanding, the focal area of this study will be the San Francisco Bay Area. The Bay Area and Central California are largely impacted by baseline O_3 which, coupled with heavy urban pollution, seasonal wildfires, and SI events, increases the frequency of non-attainment days. The quantified contribution of baseline O_3 and O_3 generated from urban precursor emissions and non-controllable sources is important to understand for future emission control planning. Therefore, the goal of this study is to examine the sources of surface urban O_3 enhancements and quantify the inland transport of baseline O_3.

2. Data and methods

2.1. Ozonesondes

On eleven dates between July and August 2018, two electrochemical concentration cell (ECC) ozonesondes were simultaneously launched from HMB and San Jose, CA (SJ) at approximately 1400 PDT (2100 UTC) (Fig. 1). This launch time was selected in order to capture peak O_3 concentrations due to the photochemical production of O_3 during the daytime. ECC ozonesondes have been deemed a reliable and accurate measurement method through laboratory and field experimental studies (e.g., Lui et al., 2009). For this study, each ozonesonde was prepped two weeks before launch and calibrated in the lab the morning of following NOAA ESRL procedures (https://www.en-sci.com/documentation/). The average uncertainties of measurements were between ±7–10% for all launches. SJ launches were conducted on the roof of Duncan Hall at an altitude of approximately 50 m above sea level (ASL) while HMB ozonesondes were launched at an elevation of roughly 9 m above sea level (ASL). O_3 mixing ratio measurements were averaged into 100 m vertical levels. Each experiment lasted around 2 h and reached an altitude of about 20 km. To focus on tropospheric O_3, only the lowest 15 km will be studied. Data below 100 m were also eliminated to account for the difference in launch altitudes between sites. Launch dates were selected based on ideal onshore wind conditions aloft (southwest to northwest winds) to ensure measurements of baseline O_3 at HMB and to represent the inland transport of the HMB airmass into the SJ region. To quantify the enhancement of O_3 in the urban profile in the absence of baseline O_3, HMB O_3 was subtracted from SJ O_3, creating what will be called the "enhancement profile" for each date. A statistical comparison between the two profiles on each date was also explored to verify that HMB can be assumed to represent baseline O_3 for SJ.

2.2. Estimating mixing layer heights

To further assess the atmospheric processes occurring at SJ, the mixing layer heights for each date over SJ were estimated using vertical profiles of relative humidity (%) and potential temperature (K) provided by the radiosonde, which is launched in tandem with the ozonesonde. Identifying the maximum gradients of relative humidity and potential temperature has been shown to be an adequate method for estimating the top of the mixing layer (Wang and Wang, 2014; Garrat, 1994; Sediel et al., 2010; Ao et al., 2008). The two variables were plotted together and altitudes where a visibly steep drop in relative humidity and an increase in potential temperature were denoted as the mixing layer top. Because this is an estimate, the mixing layer heights were also compared with the Weather Research and Forecasting (WRF) model. The North American Mesoscale Model (NAM) 6-h reanalysis data were used for the model input and the Thompson physics scheme was applied as the physics parameterization. For each launch date, a 24-h model run (0000 UTC on launch date - 0000 UTC on the day after) was conducted for a 1 km by 1 km domain covering HMB and SJ.

2.3. HYSPLIT analysis

An additional analysis was completed using the NOAA Hybrid Single-Particle Lagrangian Integrated Trajectory model (HYSPLIT) model to determine the source of the airmass at SJ and if HMB is representative of the baseline O_3 transported into the urban region. The archived Global Data Assimilation System (GDAS) 0.5° meteorology file on the date of each launch was selected for the model input. A 24-h backwards trajectory from SJ (37°19′57.78″N, 121°52′56.55″W) beginning at 2100 UTC on the launch date was run at 0.05, 5, and 10 km altitudes to capture the entire tropospheric column.

2.4. Surface, tropospheric, and total column O_3

Following the methods of David and Nair (2011), the mixing layer, tropospheric, and total column O_3 at SJ and HMB were compared using the ozonesonde and MERRA-2 single-level diagnostics, time-averaged, 1 h model (0.5° × 0.625°) (Global Modeling and Assimilation Office, 2015a). The ozonesonde provides total column O_3 measurements in Dobson Units (DU). Tropopause pressure was provided by AIRS daily 1° standard physical retrieval (AIRS Science Team/Joao Teixeira, 2013) and total column O_3 was obtained from MERRA-2, both measurements using a 0.2° by 0.2° bounding box centered on each site. Stratospheric O_3 was thereby included in the total column calculation. Mixing layer (ML) O_3 was calculated as the ozonesonde total column O_3 value at the top of the mixing layer and tropospheric O_3 was the ozonesonde total column O_3 value at the tropopause pressure given by AIRS. The percent contribution of ML to tropospheric and tropospheric to total column O_3 were then computed.

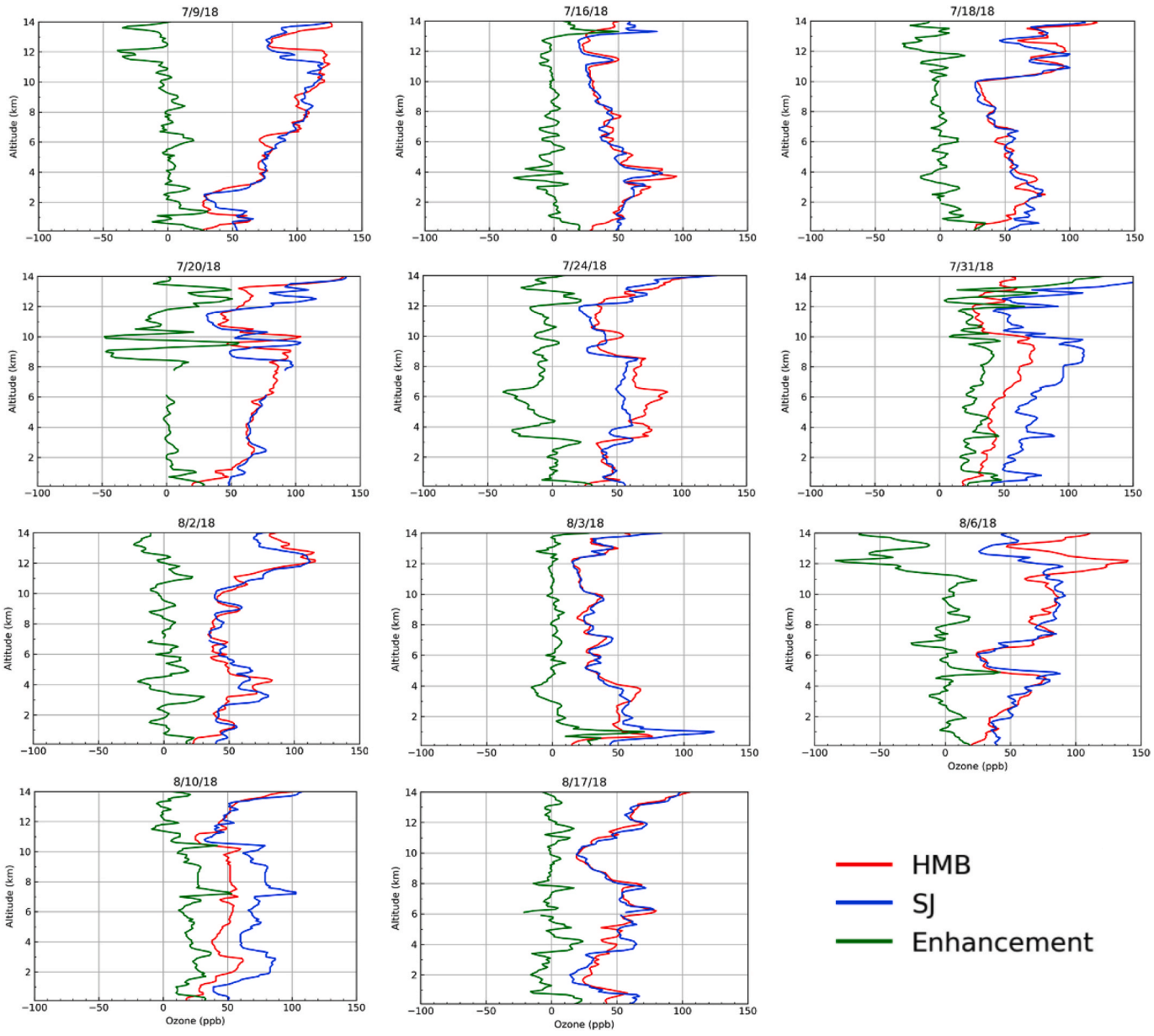

Fig. 4. Ozone profiles of HMB (red), SJ (blue) and the enhancement profile (green) from each launch. Dates are listed in Table 1. Altitude is above sea level (ASL). (For interpretation of the references to colour in this figure legend, the reader is referred to the Web version of this article.)

3. Results and discussion

3.1. HYSPLIT

The HYSPLIT back trajectories initiated at 5 km and 10 km above ground level suggested airmasses over SJ were typically transported from the SSW to NW, while the surface trajectories were mostly from NNW, passing over the San Francisco Bay region into the SJ area (Fig. 2). On dates when the upper-level trajectories did not pass over the HMB region, they typically passed the coastline 50–100 km south of HMB, which is well within synoptic and mesoscale boundaries, therefore the airmass composition is likely similar between HMB and the coastal intersection point. Wind directions have minimal differences between HMB and the coast to the south so both sites are primarily receiving onshore winds off of the Pacific. There are few urban areas within this coastal region, so it is a reasonable assumption that SJ is receiving baseline O_3 in a similar composition to HMB. Additionally, Parrish et al., (2010) (and Liu et al., 2009 therein) demonstrated that direct transport between Trinidad Head, CA and inland surface sites in the Northern Sacramento Valley is not necessary to explain observed results because the horizontal scale before correlation coefficients decrease by a factor of e is between 500 and 1000 km. As a result, the HMB concentrations are deemed applicable for the purposes of this study.

This claim was also supported by a statistical analysis between HMB and SJ on each date. Table 1 describes the correlation coefficients between HMB and SJ for the full vertical resolution from 0.1 km to 15 km (e.g. tropospheric O_3). All CCs are above the significance threshold of 0.5, with the lowest of 0.68 on August 6. The visual similarities between HMB and SJ profiles and the small values of the enhancement profile above the PBL also confirm the strong relationship between the two sites. For all dates combined, the CC was also high at 0.79. A scatter plot of SJ and HMB with a major axis regression line is shown in Fig. 3. The data followed a linear pattern, with a slope of 1.00 SJ ppb/HMB ppb, illustrating the similar O_3 concentrations between sites throughout the dataset and the underlying influence of baseline O_3 on the SJ profile.

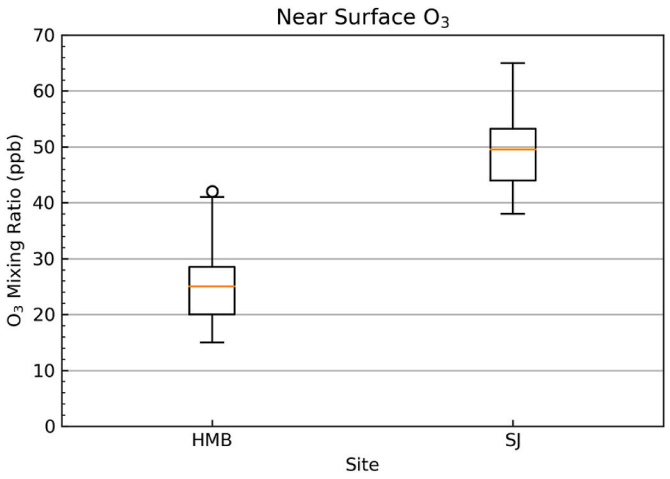

Fig. 5. Box plot of O_3 concentrations below 0.5 km at HMB and SJ. The orange line in the middle is the median value and the top and bottom lines of the box are the 75th and 25th quartiles, respectively. The top and bottom extended lines (whiskers) are the maximum and minimum values and the open circle represents an outlier. (For interpretation of the references to colour in this figure legend, the reader is referred to the Web version of this article.)

3.2. Enhancement profiles

Upon initial examination, the enhancement profiles generally did not show any significant urban enhancement of O_3 aloft (Fig. 4), indicating minimal impact of high surface urban O_3 on the tropospheric profile. Surface levels were consistently 20–30 ppb higher at SJ (Fig. 5), however above the ML, the two profiles matched closely and differences between them remained close to 0 ppbv. Near-surface HMB O_3 is consistent with observations from other surface coastal sites in northern CA (Fig. 6): within 10 ppb of the other four locations. Additionally, a potential SI was observed on August 3 and will be discussed in further sections. Smoke was visibly present near the surface on August 3, contributing to the observed spike in O_3 around 1 km.

A notable offset in O_3 concentrations aloft was observed on July 31 and August 10 (e.g., Fig. 4). While ozonesondes are a reliable measurement source, changes in model type of ECC ozonesonde or sensing solutions can induce measurement differences of up to 5–10% (e.g., Smit et al., 2007). In our cases, the same ECC ozonesonde model and solutions were used for all launches. HMB and SJ are within the same synoptic and meso spatial scales and had very similar profiles of wind speed and direction, so the consistent offset throughout the vertical profile is not attributed to differences in atmospheric conditions. It is suspected that the observed SJ enhancement on July 31 and August 10 is a result of ozonesonde discrepancies, even with the same ECC model and solution.

Local meteorological conditions were examined to investigate the enhancement of PBL O_3 at SJ and identify potential sources. Surface temperature and cloud cover data were retrieved from NOAA's Climate Data Online (CDO) local climatological data (https://www.ncdc.noaa.gov/cdo-web/datatools/lcd). The San Jose KSJC station (US WBAN: 72494523293) was selected for SJ and is located at 37.3591°N, -121.9240 °W at an elevation of 15.5 m. It is roughly 4.7 km from the SJ launch site. The Half Moon Bay airport, KHAF, (US WBAN: 72064600228) was selected for HMB and is at an elevation of 20.1 m and located at 37.5130 °N and -122.5010 °W. It is about 1.8 km from the HMB launch site.

HMB was overcast for four of the eleven days while SJ reported few clouds to clear skies each day as recorded by observations at the launch site and confirmed with the WBAN station reports. As mentioned in the introduction, increased sunlight is conducive to higher O_3 production. Additionally, surface temperatures at SJ were warmer than HMB by an average of 14.3 °C from 7/9 to 8/17. SJ also had a larger range in diurnal temperatures than HMB (Fig. 7). Low temperatures between sites were typically different by 10° but SJ high temperatures were greater by 15–25°. O_3 has been shown to increase with increasing temperatures (Dawson et al., 2006; Bloomer et al., 2009) and a plot of SJ surface temperature and surface O_3 (Fig. 8) showed similar findings with a slope of 1.08 ppb/°C and $R^2 = 0.70$. Additional studies derived similar regression line slopes for O_3 and temperature. Rasmussen et al., (2012) found slopes to be 1–3 ppb K^{-1} in the northeast U.S. in May and 4–6 ppb K^{-1} in the southeastern U.S. in May and July. Bloomer et al., (2009) found a slope of roughly 2.2 ppbv/°C in the eastern U.S. post 2002. Surface O_3 measurements were provided by the Bay Area Air Quality Management District (BAAQMD) Jackson Street site, which is located at 37.35 °N, -121.89 °W two stories above ground level. Full details of this site are included in the 2017 Air Monitoring Network Plan (Knoderer et al., 2018). Surface O_3 followed the diurnal trend of surface temperature, as well, providing further evidence of the temperature dependence on O_3 at SJ. Vertical profiles of wind speed and wind

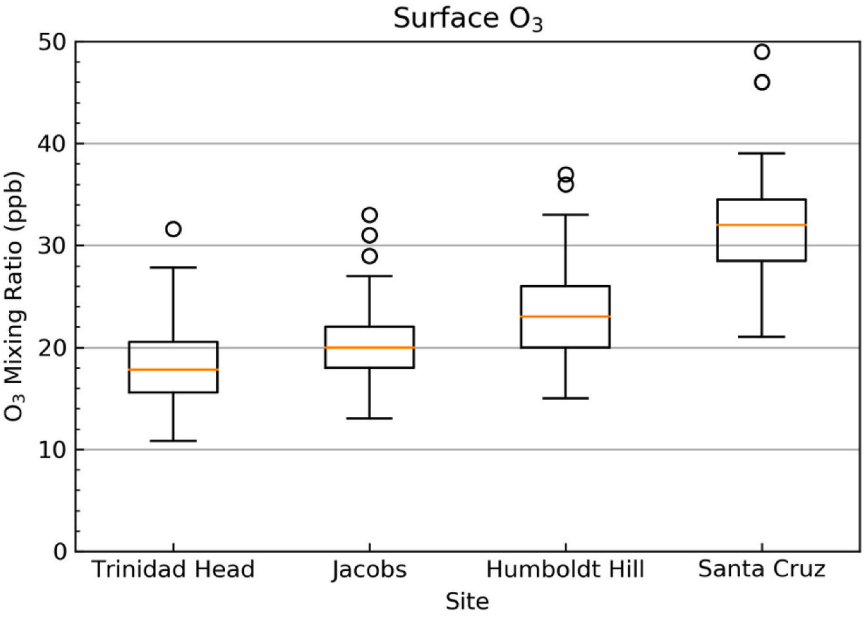

Fig. 6. Surface O_3 from four coastal sites across northern California. Data are for July and August 2018 daily averages for all hours of the day. The orange line in the middle is the median value and the top and bottom lines of the box are the 75th and 25th quartiles, respectively. The top and bottom extended lines (whiskers) are the maximum and minimum values and the open circles represent outliers. Jacobs, Humboldt Hill, and Santa Cruz are measured by EPA monitoring stations and Trinidad Head is provided by NOAA Earth System Research Laboratories (ESRL) Global Monitoring Laboratory. (For interpretation of the references to colour in this figure legend, the reader is referred to the Web version of this article.)

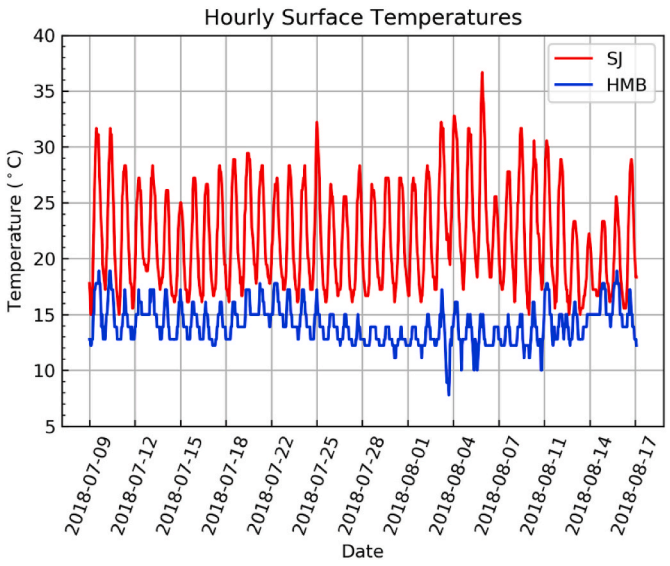

Fig. 7. Time series of surface temperatures for HMB (blue) and SJ (red). (For interpretation of the references to colour in this figure legend, the reader is referred to the Web version of this article.)

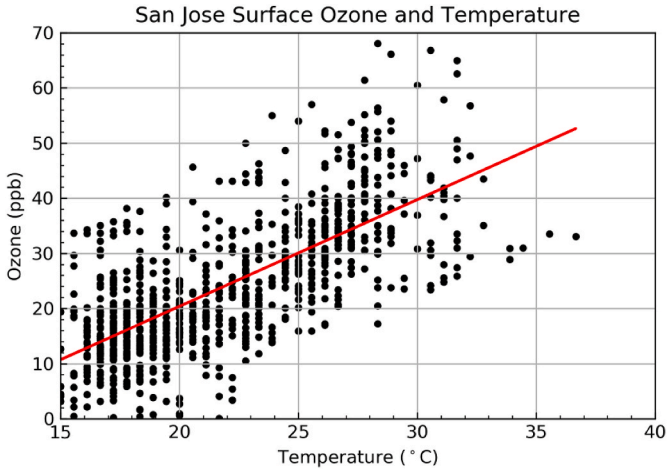

Fig. 8. Relationship between SJ surface O_3 and surface temperatures from July 9 – August 17. Best fit line equation: y = 1.08 ppb/°C * x – 53 ppb and $R^2 = 0.70$.

direction revealed similar results for both HMB and SJ so these variables can be ruled out as a cause for SJ surface enhancement.

3.3. Synoptic conditions

For most dates, low pressure was observed off of the coast of the Western U.S. with high pressure present over the southwest to western U.S. This set up of large-scale high pressure to the SE and low pressure to the N was conducive to south-westerly to westerly winds at HMB. This wind pattern is ideal for inland transport of the airmass at HMB into the SJ region and for on-shore measurement of O_3 at HMB that has not been contaminated by any local sources. Upper level wind speeds were highest on dates when these low pressure centers were observed. Lower level wind speeds were consistent between the two sites and remained around 10 ms^{-1} or below. Upper level wind speeds typically remained between 20 and 30 ms^{-1}, with the strongest winds observed on August 2 and 3 above 11 km due to a strong jet present over northern California throughout this time period. As shown in Fig. 9, three different synoptic

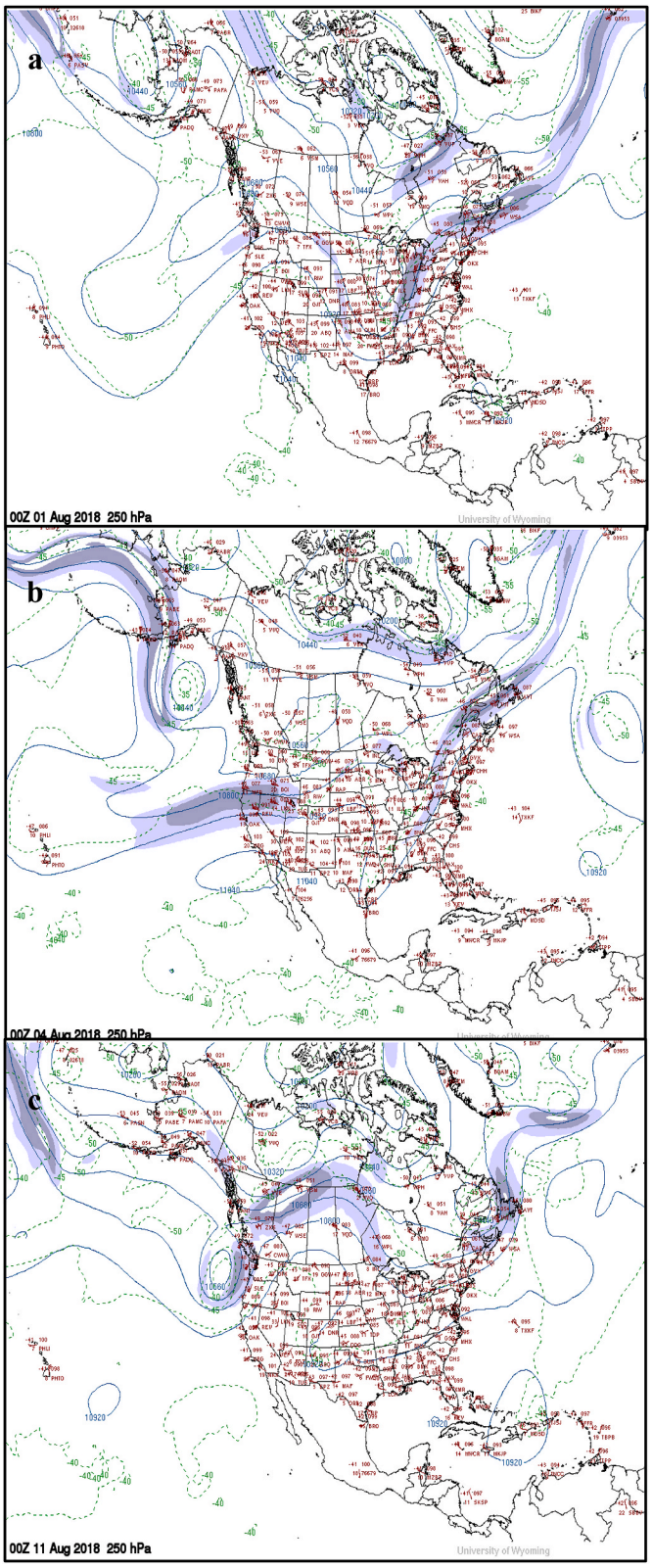

Fig. 9. 250 hPa maps for the three potential SI cases (a) 01 August, (b) 04 August, and (c) August 11, 2018 valid at 00Z. Images are provided by the University of Wyoming.

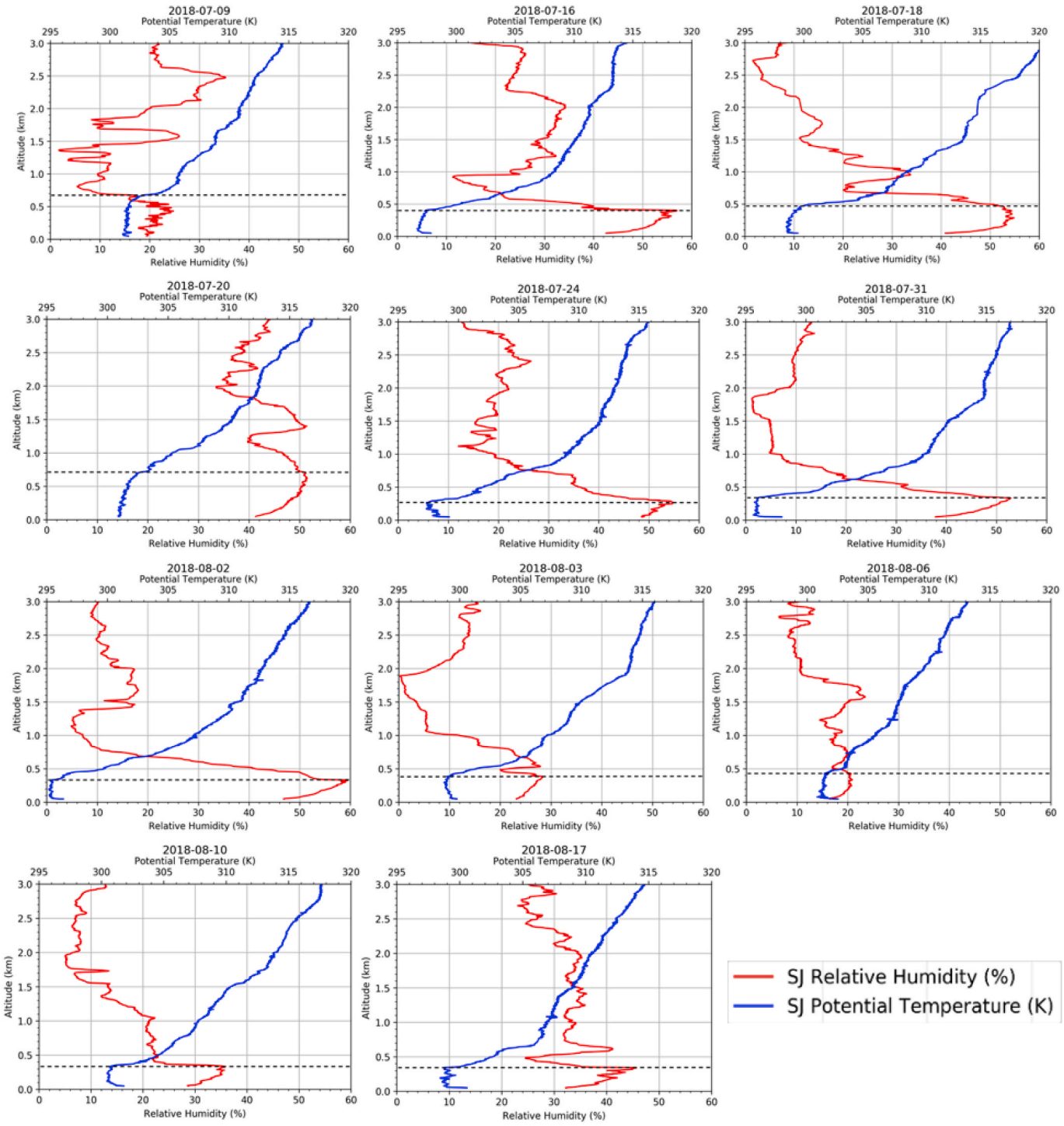

Fig. 10. Mixing layer height (m) estimations for SJ using the radiosonde observations of relative humidity and potential temperature. Note, the radiosonde is attached to and launched with the ozonesonde. At SJ, launches began at roughly 50 m above sea level (ASL) on the roof of Duncan Hall. Mixing layer height is denoted by the black dashed line.

setups will be examined in later sections for SI impacts: a positively tilted trough (July 31), low pressure center over the Gulf of Alaska coupled with a deep trough and strong jet (August 3), and a low pressure center off of the coast of the Pacific Northwest (August 10).

3.4. Mixing layer heights

The ML heights for each date were below 1 km, with 9 dates below 0.5 km (Fig. 10). The WRF planetary boundary layer heights agreed well with the radiosonde estimations, with the largest difference of 260 m on July 20. The WRF model typically under-estimated the radiosonde observations (8 out of the 11 dates produced too low mixing layer tops). However, WRF followed the general trend of observed ML heights with correlation values of $R^2 = 0.72$ (p-value = 0.01). Overall, both WRF and the radiosonde estimates observed a shallow mixing layer. These low heights reduce the extent of entrainment of tropospheric air into the boundary layer (Wigder et al., 2013), thereby reducing the vertical mixing potential of surface emissions.

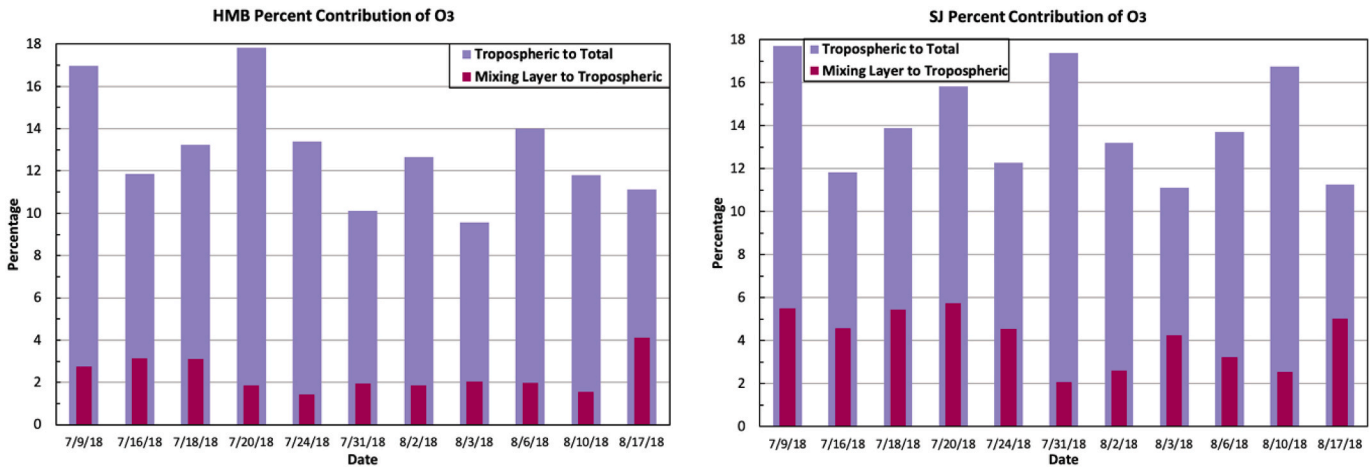

Fig. 11. Contribution of ML to tropospheric O_3 and tropospheric to total column O_3.

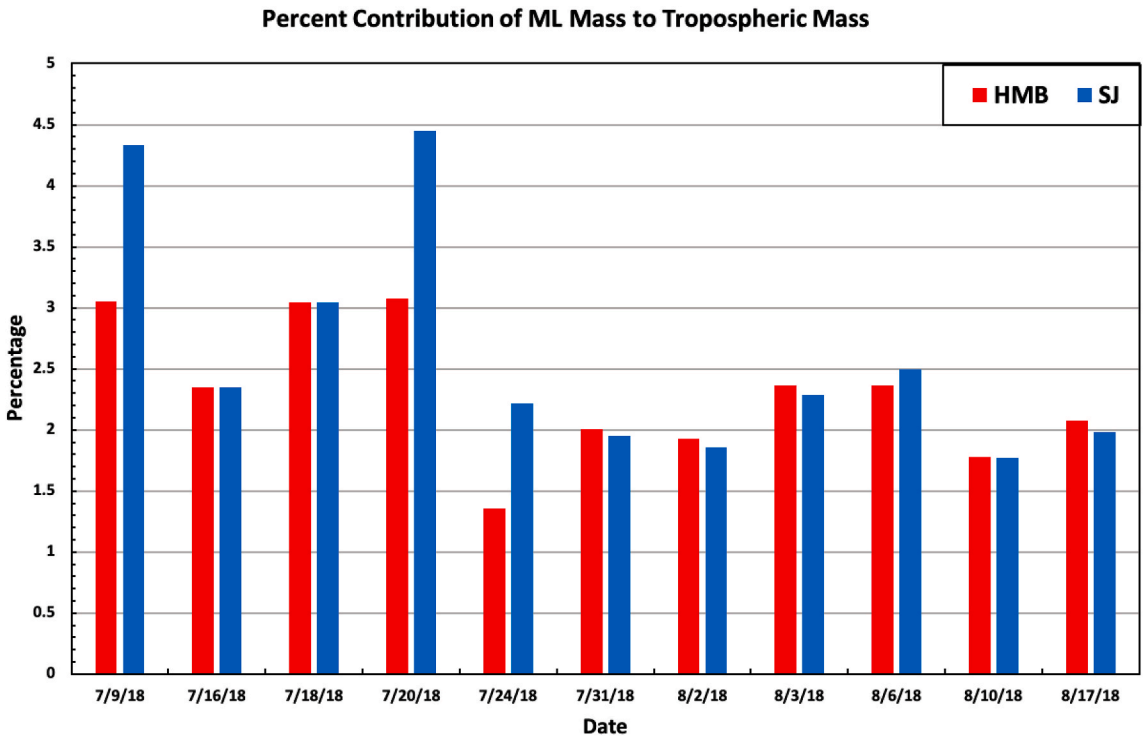

Fig. 12. Percent contribution of ML atmospheric mass per unit area (kg m^{-2}) to tropospheric mass per unit area (kg m^{-2}). HMB in red and SJ in blue. (For interpretation of the references to colour in this figure legend, the reader is referred to the Web version of this article.)

3.5. Surface, tropospheric, and total column O_3 percent contributions

ML O_3 contribution to tropospheric O_3 (Fig. 11) at both sites ranges from 2 to 6% and tropospheric to total column O_3 is 9–18%. The small contribution of ML O_3 stems from the shallow ML heights over HMB and SJ and lack of convective activity that is conducive to vertical mixing. Tropospheric contribution is comparable at both locations but ML contribution is consistently higher at SJ because of local urban pollution leading to higher near surface O_3. However even with increases in surface O_3 by 20–30 ppb from HMB to SJ, the SJ ML O_3 impact on tropospheric O_3 is still very low, roughly 1–4% higher than HMB. Furthermore, there does not appear to be a relationship between the percent of ML O_3 contribution on tropospheric O_3 and the contribution of tropospheric O_3 to total column O_3. On July 31 at SJ, ML O_3 contribution decreased while tropospheric increased and from August 2 to 3, the ML increased to roughly 4.1% while tropospheric decreased. July 9 had the highest tropospheric contribution, with the next highest on July 31. However, the ML contribution was the lowest on July 31. The ML O_3 does not appear to be indicative of tropospheric O_3 patterns at either location.

Similarly, the atmospheric mass contributions for ML to tropospheric were compared at each location using the following equation (1) to compute the mass of the ML column and the tropospheric column,

$$m = \int_0^{\infty} \rho dz \tag{1}$$

where m = mass per unit area (kg m^{-2}), $\rho = 1.2$ kg m^{-3} (e.g. an estimated average density of the atmosphere), and dz = change in altitude from launch to top of ML (m) and launch to tropopause (m). For both sites and all dates, ML mass contributes about 1.3–4.5% to the tropospheric mass

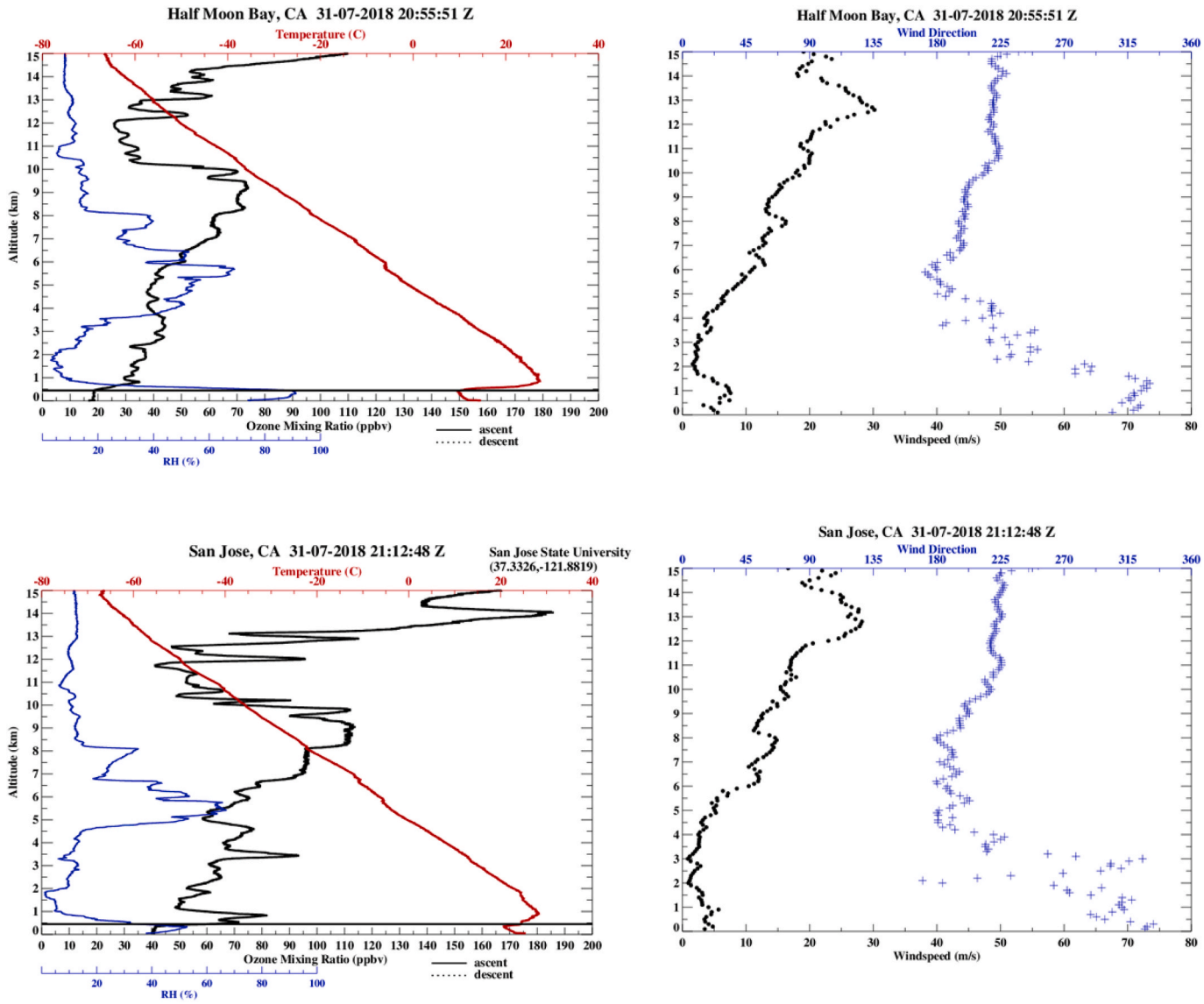

Fig. 13. July 31 profiles for HMB (top) and SJ (bottom). Horizontal black line in the left figures denote potential SI altitude.

(Fig. 12). SJ ML contribution was higher for three of the eleven dates but the two sites were comparable for the rest of the launches. The limited contribution of ML mass agrees with the low ML O_3 percent contributions to the tropospheric column. The stability of the atmosphere in this region limits the growth of the ML and entrainment of ML O_3 into the free troposphere and, consequently, limits the long-range transport of high surface urban O_3. These results further emphasize the importance of understanding baseline O_3; even over urban SJ, baseline O_3 remains the dominant influence on the tropospheric column.

3.6. Stratospheric intrusions (SI) cases

Indications of a potential SI via a steep drop in RH with an increase in O_3 were identified on July 31, August 3, and August 10 from Figs. 13–15, respectively. To further investigate the SI, the potential vorticity (PV) using NASA MERRA-2 data was analyzed at lower levels (~ 925 hPa) to determine if stratospheric air was present over the region (Fig. 16) (Global Modeling and Assimilation Office, 2015b). Common dynamic tropopause height has been identified as the 2 PVU isosurface (Sprenger et al., 2007; Martius et al., 2010; Clark and Chiao, 2019) and will be used in this study to indicate stratospheric air. A backwards HYSPLIT trajectory originating from the SJ site was used to determine if there was strong vertical descent of air into the region (Fig. 17). Each trajectory was initialized at 2100 UTC on the date of each launch from SI altitudes: 0.5 km on July 31, 1 km on August 3, and 1 km on August 10. To further confirm stratospheric influence following the methods of Ryoo et al., (2017), a scatter plot analysis was conducted between relative humidity and O_3 (Fig. 18).

The results showed that only July 31 had PV greater than 2.25 PVU off the coast of California at 950 hPa, indicating air of stratospheric origin (Fig. 16). The highest O_3 concentrations were also present at low RH and the backwards trajectory showed a descent from 11 km over the course of a week with a steeper descent over the days before (Fig. 17). It is important to note that winds below 4–5 km on all dates were from the north, potentially advecting polluted air from the San Francisco region into HMB and SJ and increasing O_3. This cannot be ruled out as a contribution to higher concentrations on July 31 in addition to an SI.

A large spike in O_3 occurred at roughly 1.0 km on August 3 (Fig. 13). RH less than 40% was present at all altitudes over SJ (Fig. 13). Additionally, the backwards HYSPLIT did not show a descent from stratospheric altitudes (Fig. 17). The MODIS image of day and night fire and thermal anomalies from August 2 demonstrated several locations of wildfires in Northern California (Fig. 19). Wildfire smoke is a significant source of O_3 precursors, such as CO, NO_x, and VOCs. As a result, these

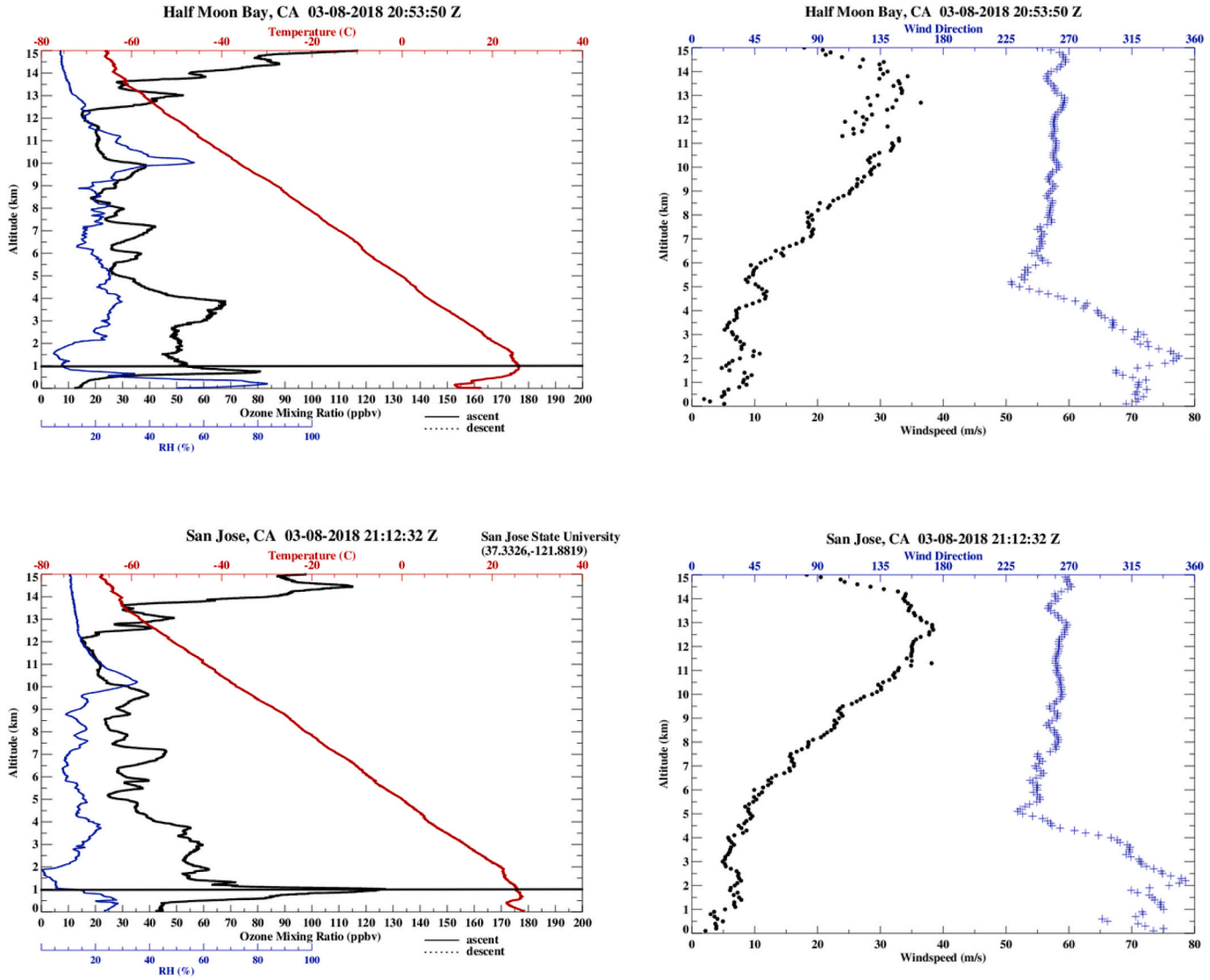

Fig. 14. August 3 profiles for HMB (top) and SJ (bottom). Horizontal black line in the left figures denote potential SI altitude.

plumes can increase surface O_3 downwind due to advected elevated O_3 concentrations produced within the plumes (Lindaas et al., 2017; Pfister et al., 2008). This, coupled with PV ~ 1.5 PVU and northerly winds in the lowest 5 km indicate the dry, O_3-rich air is a result of advected wildfire smoke and polluted urban air and not an SI.

August 10 had a similar HYSPLIT descent as July 31 but from a lower altitude and the PV (at 900 hPa) is low on this date (Fig. 16). There are high O_3 concentrations with low RH (Fig. 18). However, winds are coming from the north to northeast, bringing in dry continental air (Fig. 15). Additionally, polluted urban air from the north, as with July 31, can be a cause for increased O_3 on this date. Because of these variables, it is determined that an SI did not occur on August 10.

4. Conclusion

This study investigated the impact of non-controllable sources on O_3 enhancements and the influence of inland transported baseline O_3. An enhancement profile was created to describe the enhancement of O_3

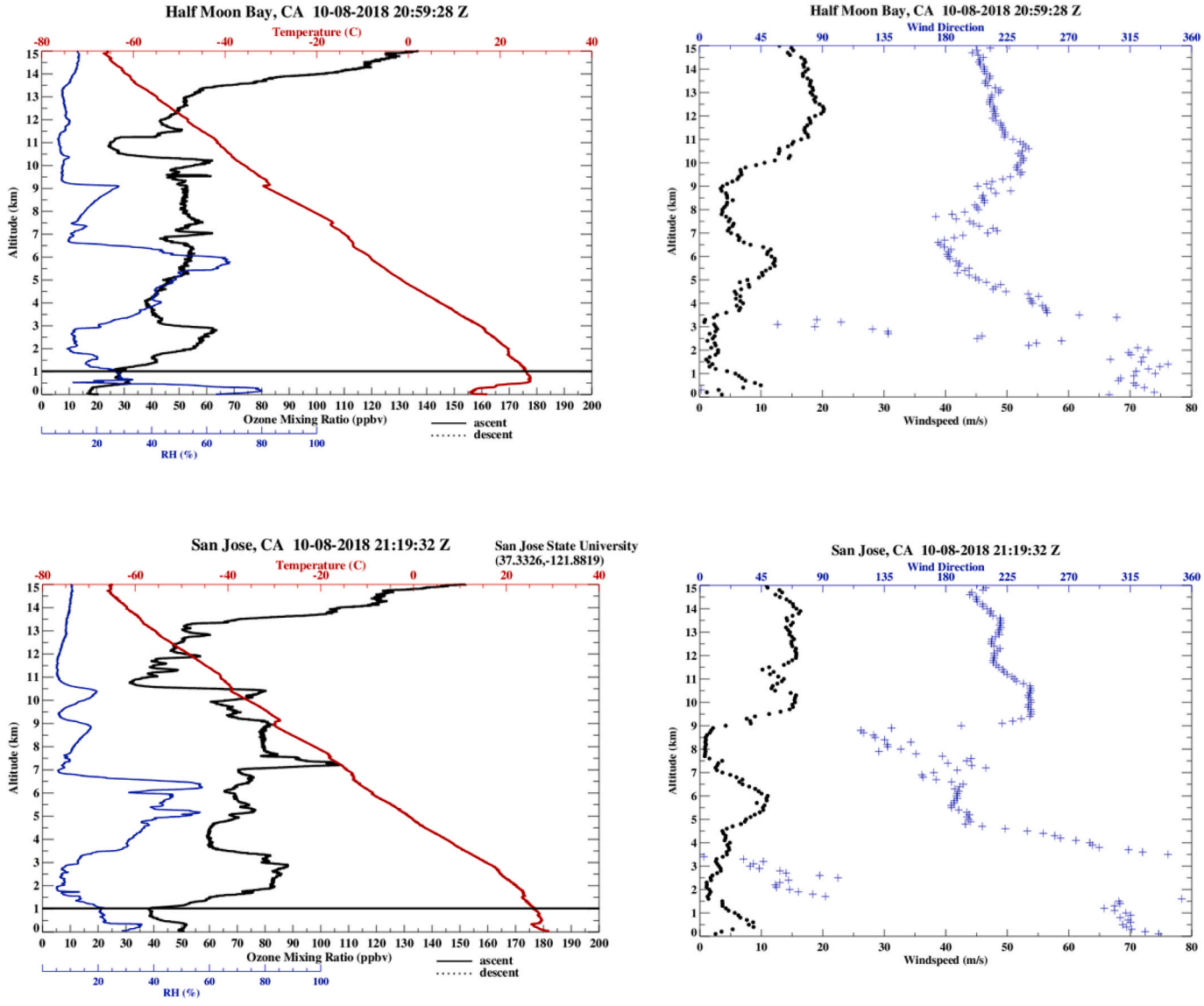

Fig. 15. August 10 profiles for HMB (top) and SJ (bottom). Horizontal black line in the left figures denote potential SI altitude.

over SJ by subtracting out the HMB baseline O_3 profile. Surface O_3 at SJ was higher than HMB by roughly 20–30 ppb for all dates and can be attributed to higher surface temperatures and higher concentrations of O_3 precursors.

Anomalies occurred on July 31, August 3, and August 10 and were examined to identify potential SIs. Synoptic conditions on all dates were conducive to SIs but only July 31 was observed to have stratospheric air increasing O_3 concentrations in the profile, characterized by low relative humidity, high PV, and vertical descent of air into the region leading up to launch. August 3 was impacted by residual smoke from wildfires in northern California, as confirmed by backwards trajectories passing over the northern state, winds originating from the north in the lower vertical profile, and MODIS observed smoke plumes across northern California. RH was less than 40% for all altitudes, indicating dry, O_3-rich air typical

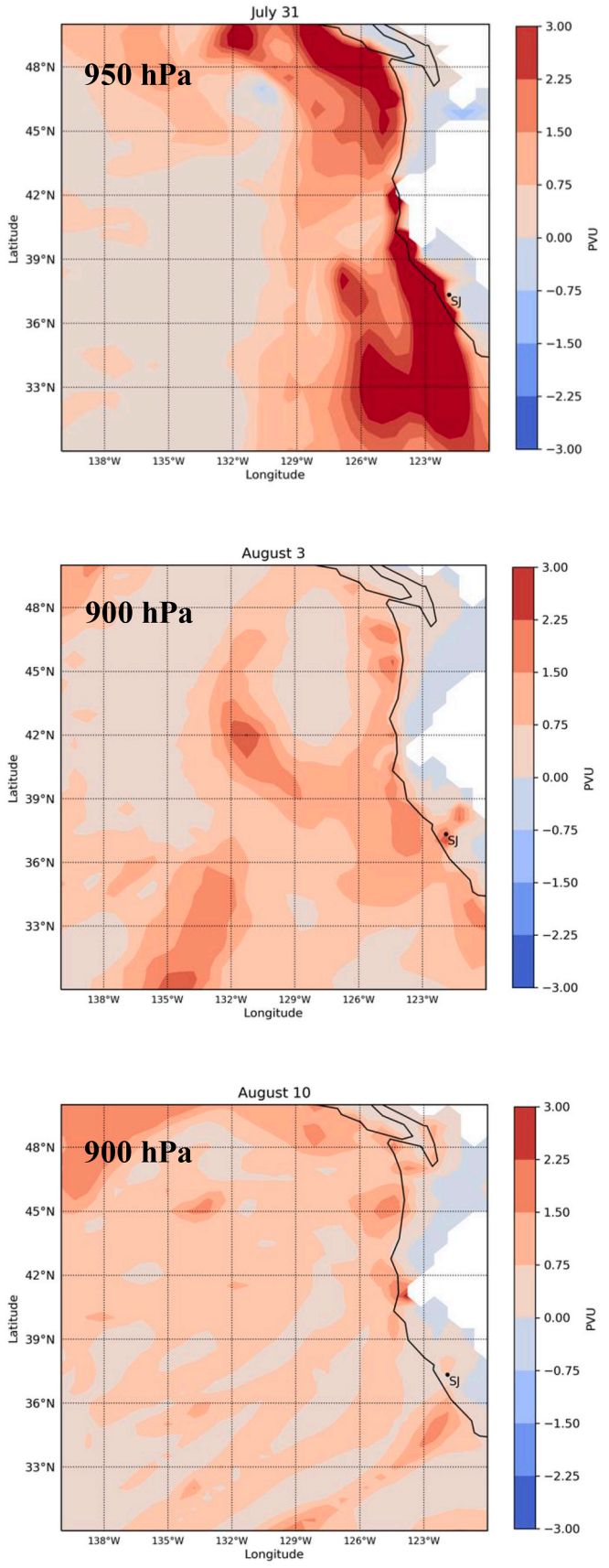

Fig. 16. MERRA-2 potential vorticity (PV) plotted at SI pressure levels at 950 hPa on July 31, 900 hPa on August 3, and 900 hPa on August 10.

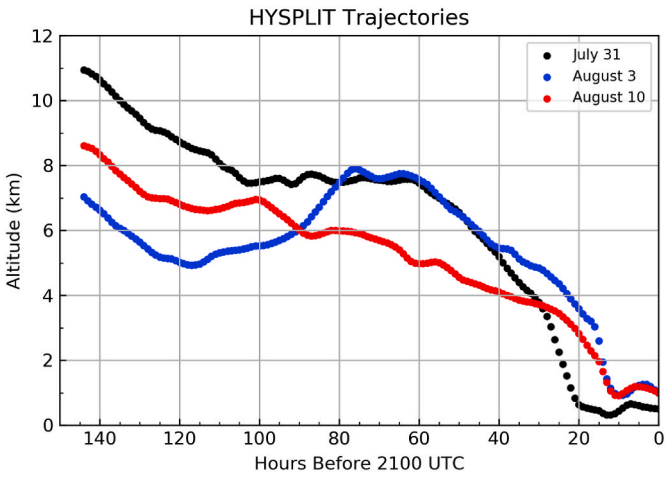

Fig. 17. Backwards HYSPLIT trajectories for potential SI dates.

of wildfire plumes. August 10 was not observed to be stratospherically influenced, evidenced by low PV over the region.

The processes that control O_3 production and transport are fairly large scale, so it is expected that HMB and SJ are strongly related above the ML. The major axis regression had a slope of 1.00 SJ ppb/HMB ppb and intercept of 0.004 ppb; SJ O_3 followed closely to HMB. The two sites were strongly correlated, with R^2 values ranging from 0.68 to 0.93. Furthermore, SJ ML O_3 had minimal contributions to observed tropospheric O_3 of only 2–6%. Despite surface O_3 increases from HMB to SJ, the contribution of ML O_3 to tropospheric O_3 at SJ only increased by about 1–4%.

The results of this study indicate the importance of understanding baseline O_3 in the western U.S. For central California, which is susceptible to high pollution events due to low mixing layer heights keeping pollutants close to the surface and inhibiting vertical mixing, baseline O_3 remains the predominant influence on free and upper tropospheric O_3. While high surface O_3 episodes are important to understand, free tropospheric O_3 has a longer lifetime than O_3 within the ML and can be transported over large distances as well as entrained into the PBL, further contributing to these episodes. High O_3 concentrations in the free troposphere can also be transported from other continents, thereby increasing baseline O_3 concentrations and contributing to exceedances in the western U.S. Consequently, as urban emissions decrease with improved controls, upper level O_3 concentrations remain largely influenced by baseline O_3 trends and can impact surface concentrations, which presents a unique challenge for remaining within the NAAQS for O_3. Additionally, it would be useful to incorporate modeling studies to further assess vertical transport processes in inland urban regions in the western U.S., as well as investigate the inland transport of baseline O_3 from the coast further inland into California to supplement existing literature.

Declaration of interest statement

We the undersigned declare that this manuscript is original, has not been published before and is not currently being considered for publication elsewhere.

We wish to confirm that there are no known conflicts of interest associated with this publication and there has been no significant financial support for this work that could have influenced its outcome.

We confirm that the manuscript has been read and approved by all named authors and that there are no other persons who satisfied the criteria for authorship but are not listed. We further confirm that the order of authors listed in the manuscript has been approved by all of us.

We confirm that we have given due consideration to the protection of intellectual property associated with this work and that there are no

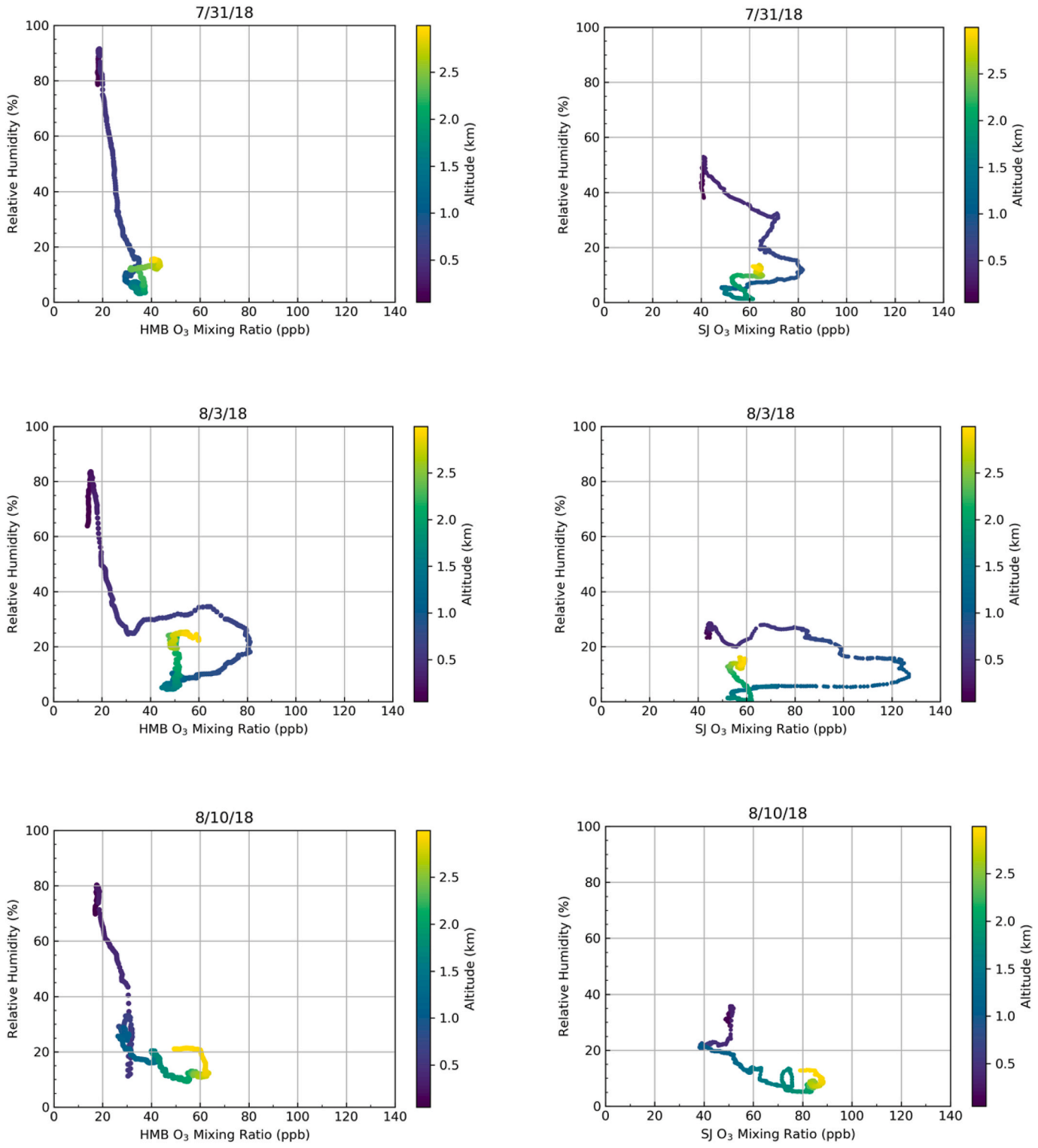

Fig. 18. Scatter plots of relative humidity and O_3 for HMB (left) and SJ (right).

impediments to publication, including the timing of publication, with respect to intellectual property. In so doing we confirm that we have followed the regulations of our institutions concerning intellectual property.

We understand that the Corresponding Author is the sole contact for the Editorial process (including Editorial Manager and direct communications with the office). He is responsible for communicating with the other authors about progress, submissions of revisions and final approval of proofs. We confirm that we have provided a current, correct email address which is accessible by the Corresponding Author and which has been configured to accept email from aea@elsevier.com.

CRediT authorship contribution statement

Chloe Gore: Conceptualization, Methodology, Validation, Resources, Writing - original draft, Writing - review & editing. **Sen Chiao:**

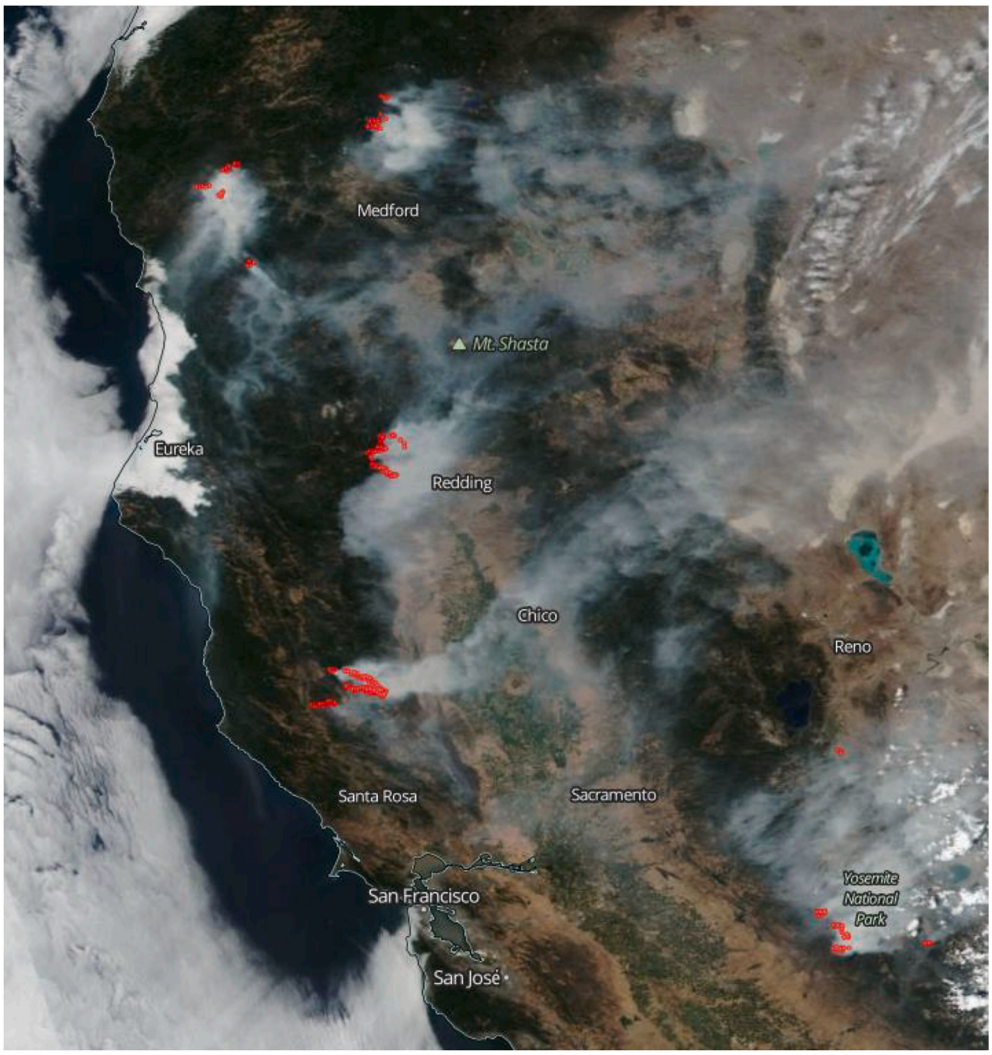

Fig. 19. NASA EOSDIS Worldview MODIS image of day and night fire and thermal anomalies from August 2.

Conceptualization, Methodology, Validation, Resources, Writing - review & editing.

Declaration of competing interest

The authors declare that they have no known competing financial interests or personal relationships that could have appeared to influence the work reported in this paper.

Acknowledgements

We acknowledge the suppliers of datasets utilized in this research. We wish to express our appreciation to Drs. Jin Xu and Matthew Johnson for the suggestions for the development of this research. This research was supported by the NASA MUREP # NNX15AQ02A. The research is based on the thesis research of the first author and repeated in this paper with permission.

Appendix A. Supplementary data

Supplementary data to this article can be found online at https://doi.org/10.1016/j.aeaoa.2020.100085.

References

AIRS Science Team/Joao Teixeira, 2013. AIRS/Aqua L3 Daily Standard Physical Retrieval (AIRS-only) 1 degree x 1 degree V006. Goddard Earth Sciences Data and Information Services Center (GES DISC), Greenbelt, MD, USA. https://doi.org/10.5067/Aqua/AIRS/DATA303. Accessed: June 8, 2020.

Anenberg, S.C., Horowitz, L.W., Tong, D.Q., West, J.J., 2010. An estimate of the global burden of anthropogenic ozone and fine particulate matter on premature human mortality using atmospheric modeling. Environ. Health Perspect. 118, 1189–1195. https://doi.org/10.1289/ehp.0901220.

Ao, C., Chan, T., Iijima, B., Li, J., Mannucci, A., Teixeira, J., Tian, B., Waliser, D., 2008. Planetary boundary layer information from GPS radio occultation measurements. In: GRAS SAF Workshop on Applications of GPSRO Measurements, 2008, pp. 123–131.

Avnery, S., Mauzerall, D.L., Lui, J., Horowitz, L.W., 2011a. Global crop yield reductions due to surface ozone exposure: 1. Year 2000 potential crop production losses and economic damage under two scenarios of O_3 production. Atmos. Environ. 45, 2284–2296. https://doi.org/10.1016/j.atmosenv.2010.11.045.

Avnery, S., Mauzerall, D.L., Lui, J., Horowitz, L.W., 2011b. Global crop yield reductions due to surface ozone exposure: 2. Year 2030 potential crop production losses and economic damage under two scenarios of O_3 production. Atmos. Environ. 45, 2297–2309. https://doi.org/10.1016/j.atmosenv.2011.01.002.

Baylon, P.M., Jaffe, D.A., Pierce, R.B., Gustin, M.S., 2016. Interannual variability in baseline ozone and its relationship to surface ozone in the western U.S. Environ. Sci. Technol. 50, 2994–3001. https://doi.org/10.1021/acs.est.6b00219.

Bell, M.L., Peng, R.D., Dominici, F., 2006. The exposure-response curve for ozone and risk of mortality and the adequacy of current ozone regulations. Environ. Health Perspect. 114, 532–536. https://doi.org/10.1289/ehp.8816.

Berman, J.D., Fann, N., Hollingsworth, J.W., Pinkerton, K.E., Rom, W.N., Szema, A.M., Breysse, P.N., White, R.H., Curriero, F.C., 2012. Health benefits from large-scale ozone reduction in the United States. Environ. Health Perspect. 120, 1404–1410. https://doi.org/10.1289/ehp.1104851.

Bloomer, B.J., Stehr, J.W., Piety, C.A., Salawitch, R.J., Dickerson, R.R., 2009. Observed Relationships of ozone air pollution with temperature and emissions. Geophys. Res. Lett. 36 https://doi.org/10.1029/2009GL037308.
Chin, M., Jacob, D.J., Munger, J.W., Parrish, D.D., Doddridge, B.G., 1994. Relationship of ozone and carbon monoxide over North America. J. Geophys. Res. Atmos. 99, 14565–14573. https://doi.org/10.1029/94JD00907.
Clark, J., Chiao, S., 2019. A case study of stratospheric ozone transport to the northern san Francisco Bay area and Sacramento Valley during CABOTS 2016. J. Appl. Meteor. Climatol. 58, 2675–2697. https://doi.org/10.1175/JAMC-D-18-0322.1.
Cooper, O.R., et al., 2010. Increasing springtime ozone mixing ratios in the free troposphere over western North America. Nature 463, 344–348. https://doi.org/10.1038/nature08708.
Cooper, O.R., et al., 2011. Measurement of western US baseline ozone from the surface to the tropopause and assessment of downwind impact regions. J. Geophys. Res. 116, D00v03. https://doi.org/10.1029/2011JD016095.
Cooper, O.R., Gao, R., Tarasick, D., Leblanc, T., Sweeney, C., 2012. Long-term ozone trends at rural ozone monitoring sites across the United States, 1990-2010. J. Geophys. Res. 117, D22307 https://doi.org/10.1029/2012JD018261.
Cooper, O.R., Langford, A.O., Parrish, D.D., Fahey, D.W., 2015. Challenges of a lowered U.S. ozone standard. Science 348 (6239), 1096–1097. https://doi.org/10.1126/science.aaa5748.
Croes, B.E., M Fujita, E., 2003. The 1997 southern California ozone study (SCOS97-NARSTO): introduction and perspective. Atmos. Environ. 37 (Suppl. 2), S3–S26. https://doi.org/10.1016/S1352-2310(03)00378-9.
David, L.M., Nair, P.R., 2011. Diurnal and seasonal variability of surface ozone and NO_x at a topical coastal site: association with mesoscale and synoptic meteorological conditions. J. Geophys. Res. 116 https://doi.org/10.1029/2010JD015076.
Dawson, J.P., Adams, P.J., Pandis, S.N., 2006. Sensitivity of ozone to summertime climate in the eastern USA: a modeling case study. Atmos. Environ. 41, 1494–1511. https://doi.org/10.1016/j.atmosenv.2006.10.033.
Dentener, F., Stevenson, D., Cofala, J., Mechler, R., Amann, M., Bergamaschi, P., Raes, F., Derwent, R., 2005. The impact of air pollutant and methane emission controls on tropospheric ozone and radiative forcing: CTM calculations for the period 1990-2030. Atmos. Chem. Phys. 5, 1731–1755. https://doi.org/10.5194/acp-5-1731-2005.
Dodman, D., 2011. Forces driving urban greenhouse gas emissions. Curr. Opin. Environ. Sustain. 3, 121–125. https://doi.org/10.1016/j.cosust.2010.12.013.
Ellingsen, K., et al., 2008. Global ozone and air quality: a multi-model assessment of risks to human health and crops. Atmos. Chem. Phys. Discuss. 8, 2163–2223. https://doi.org/10.5194/acpd-8-2163-2008.
Environmental Protection Agency, 2015. National ambient air quality standards for ozone. Fed. Regist. 80, 65292–65468 available at. https://www.gpo.gov/fdsys/pkg/FR-2015-10-26/pdf/2015-26594.pdf.
Fiore, A.M., Jacob, D.J., Field, B.D., Streets, D.G., Fernandes, S.D., Jang, C., 2002. Linking ozone pollution and climate change: the case for controlling methane. Geophys. Res. Lett. 29 https://doi.org/10.1029/2002GL015601, 25-1-25-4.
Fishman, J., Seiler, W., 1983. Correlative nature of ozone and carbon monoxide in the troposphere: implications for the tropospheric ozone budget. J. Geophys. Res. Ocean 88, 3662–3670. https://doi.org/10.1029/JC088iC06p03662.
Garrat, J.R., 1994. Review: the atmospheric boundary layer. Earth Sci. Rev. 37, 89–134.
Gilge, S., Plass-Duelmer, C., Fricke, W., Kaiser, A., Ries, L., Buchmann, B., Steinbacher, M., 2010. Ozone, carbon monoxide and nitrogen oxides time series at four apline GAW mountain stations in central Europe. Atmos. Chem. Phys. 10, 12295–12316. https://doi.org/10.5194/acp-10-12295-2010.
Global Modeling and Assimilation Office (GMAO), 2015a. MERRA-2 tavg1_2d_slv_Nx: 2d,1-Hourly,Time-Averaged,Single-Level,Assimilation,Single-Level Diagnostics V5.12.4. Goddard Earth Sciences Data and Information Services Center (GES DISC), Greenbelt, MD, USA. https://doi.org/10.5067/VJAFPLI1CSIV. Accessed: June 8, 2020.
Global Modeling and Assimilation Office (GMAO), 2015b. MERRA-2 inst3_3d_asm_Np: 3d, 3-Hourly, Instantaneous, Pressure-Level, Assimilation, Assimilated Meteorological Fields V5. 12.4. Goddard Earth sciences data and information services center (GES DISC), Greenbelt, MD, USA. https://doi.org/10.5067/3Z173KIE2TPD. Accessed: March 17, 2020.
Goldstein, A.H., Millet, D.B., McKay, M., Jaeglé, L., Horowitz, L., Cooper, O., Hudman, R., Jacob, D.J., Oltmans, S., Clarke, A., 2004. Impact of asian emissions on observations at Trinidad Head, California, during ITCT 2K2. J. Geophys. Res. 109, D23S17. https://doi.org/10.1029/2003JD004406.
Gorai, A.K., Tuluri, F., Tchounwou, P.B., Ambinakudige, S., 2015. Influence of local meteorology and NO_2 conditions on ground-level ozone concentrations in the eastern part of Texas, USA. Air Qual. Atmos. Health 8, 81–96. https://doi.org/10.1007/s11869-014-0276-5.
Grewe, V., Dahlmann, K., Matthes, S., Steinbrecht, W., 2012. Attributing ozone to NO_x emissions: implications for climate mitigation measures. Atmos. Environ. 59, 102–107. https://doi.org/10.1016/j.atmosenv.2012.05.002.
Hudman, et al., 2004. Ozone production in transpacific Asian pollution plumes and implications for ozone air quality in California. J. Geophys. Res. 109 https://doi.org/10.1029/2004JD004974.
Jaffe, D., Price, H.U., Parrish, D.D., Goldstein, A., Harris, J., 2003. Increasing background ozone during spring on the west coast of North America. Geophys. Res. Lett. 30 https://doi.org/10.1029/2003GL017024.
Jaffe, D., Ray, J., 2007. Increase in surface ozone at rural sites in the western US. Atmos. Environ. 41, 5452–5463. https://doi.org/10.1016/j.atmosenv.2007.02.034.
Jaffe, D.A., Cooper, O.R., Fiore, A.M., Henderson, B.H., Tonnesen, G.S., Russell, A.G., Henze, D.K., Langford, A.O., Lin, M., Moore, T., 2018. Scientific assessment of background ozone over the U.S.: implications for air quality management. Elem. Sci. Anth. 6 https://doi.org/10.1525/elementa.309.
John, J. C. St, Chameides, W.L., Saylor, R., 1998. Role of anthropogenic NO_x and VOC as ozone precursors: a case study from the SOS Nashville/Middle Tennessee Ozone Study. J. Geophys. Res. 103 (22), 415–422. https://doi.org/10.1029/98JD00973, 423.
Konovalov, I.B., 2002. Application of neural networks for studying nonlinear relationships between ozone and its precursors. J. Geophys. Res.: Atmos. 107 https://doi.org/10.1029/2001JD000863. ACH 8-1-ACH 8-14.
Knoderer, C., Nguyen, D., Alrick, D., 2018. 2017 air monitoring Network plan. available at. http://www.baaqmd.gov/~/media/files/technical-services/2017_network_plan_20180701-pdf.pdf?la=en.
Langford, A.O., Senff, C.J., Alvarez II, R.J., Brioude, J., Cooper, O.R., Holloway, J.S., Lin, M.Y., Marchbanks, R.D., Pierce, R.B., Sandberg, S.P., Weickmann, A.M., Williams, E.J., 2015. An overview of the 2013 Las Vegas Ozone Study (LVOS): impact of stratospheric intrusions and long-range transport on surface air quality. Atmos. Environ. 109, 305–322. https://doi.org/10.1016/j.atmosenv.2014.08.040. https://search.crossref.org/?q=Langford%2C+A.+O.%2C+Senff%2C+C.+J.%2C+Alvarez+II%2C+R.+J.%2C+Brioude%2C+J.%2C+Cooper%2C+O.+R.%2C+Holloway%2C+J.+S.%2C+Lin%2C+M.+Y.%2C+Marchbanks%2C+R.+D.%2C+Pierce%2C+R.+B.%2C+Sandberg%2C+S.+P.%2C+Weickmann%2C+A.+M.%2C+and+Williams%2C+E.+J.+%282015%29%2C+An+overview+of+the+2013+Las+Vegas+Ozone+Study+%28LVOS%29%3A+impact+of+stratospheric+intrusions+and+long-range+transport+on+surface+air+quality.+Atmos.+Environ.%2C+109%2C+305-322.
Langford, A.O., Alvarez II, R.J., Brioude, J., Fine, R., Gustin, M.S., Lin, M.Y., Marchbanks, R.D., Pierce, R.B., Sandberg, S.P., Senff, C.J., Weickmann, A.M., Williams, E.J., 2017. Entrainment of stratospheric air and Asian pollution by the convective boundary layer in the southwestern U.S. J. Geophys. Res. 122 https://doi.org/10.1002/2016JD025987.
Langford, A.O., Alvarez II, R.J., Brioude, J., Evan, S., Iraci, L.T., Kirgis, G., Kuang, S., Leblanc, T., Newchurch, M.J., Pierce, R.B., Senff, C.J., Yates, E.L., 2018. Coordinated profiling of stratospheric intrusions and transported pollution by the tropospheric ozone lidar Network (TOLNet) and NASA alpha jet experiment (AJAX): observations and comparison to HYSPLIT, RAQMS, and FLEXPART. Atmos. Environ. 174, 1–14. https://doi.org/10.1016/j.atmosenv.2017.11.031.
Lefohn, A.S., Shadwick, D., Oltmans, S.J., 2010. Characterizing changes in surface ozone levels in metropolitan and rural areas in the United States for 1980−2008 and 1994−2008. Atmos. Environ. 2010 44 (39), 5199–5210.
Lindaas, J., Farmer, D.K., Pollack, I.B., Abeleira, A., Flocke, F., Roscioli, R., Herndon, S., Fischer, E.V., 2017. Changes in ozone and precursors during two aged wildfire smoke events in the Colorado Front Range in summer 2015. Atmos. Chem. Phys. 17, 10691–10707. https://doi.org/10.5194/acp-17-10691-2017.
Lin, M., Fiore, A.M., Cooper, O.R., Horowitz, L.W., Langford, A.O., Levy II, H., Johnson, B.J., Naik, V., Oltmans, S.J., Senff, C.J., 2012. Springtime high surface ozone events over the western United States: quantifying the role of stratospheric intrusions. J. Geophys. Res. 117 https://doi.org/10.1029/2012JD018151.
Lin, M., Fiore, A.M., Horowitz, L.W., Langford, A.O., Oltmans, S.J., Tarasick, D., Rieder, H.E., 2015a. Climate variability modulates western US ozone air quality in spring via deep stratospheric intrusions. Nat. Commun. 6 https://doi.org/10.1038/ncomms8105.
Lin, M., Horowitz, L.W., Cooper, O.R., Tarasick, D., Conley, S., Iraci, L.T., Johnson, B., Leblanc, T., Petropavlovskikh, I., Yates, E.L., 2015b. Revisiting the evidence of increasing springtime ozone mixing ratios in the free troposphere over western North America. Geophys. Res. Lett. 42, 8719–8728. https://doi.org/10.1002/2015GL065311.
Lin, M., Horowitz, L.W., Payton, R., Fiore, A.M., Tonnesen, G., 2017. US surface ozone trends and extremes from 1980 to 2014: quantifying the roles of rising Asian emissions, domestic controls, wildfires, and climate. Atmos. Chem. Phys. 17, 2943–2970. https://doi.org/10.5194/acp-17-2943-2017.
Logan, J.A., et al., 2012. Changes in ozone over Europe: analysis of ozone measurements from sondes, regular aircraft (MOZAIC) and alpine surface sites. J. Geophys. Res. 117, D09301. https://doi.org/10.1029/2011JD016952.
Lui, G., Tarasick, D.W., Fioletov, V.E., Sioris, C.E., Rochon, Y.J., 2009. Ozone correlation lengths and measurement uncertainties from analysis of historical ozonesonde data in North America and Europe. J. Geophys. Res.: Atmos. 114 https://doi.org/10.1029/2008/JD010576.
Macdonald, A.M., Anlauf, K.G., Leaitch, W.R., Chan, E., Tarasick, D.W., 2011. Interannual varaiability of ozone and carbon monoxide at the Whistler high elevation site: 2002-2006. Atmos. Chem. Phys. 11, 11431–11446. https://doi.org/10.5194/acp-11-11431-2011.
Marcotullio, P.J., Sarzynski, A., Albrecht, J., Schulz, N., Carcia, J., 2013. The geography of global urban greenhouse gas emissions: an exploratory analysis. Clim. Change 121, 621–634. https://doi.org/10.1007/s10584-013-0977-z.
Martius, O., Schwierz, C., Davies, H.C., 2010. Tropopause-level waveguides. J. Atmos. Sci. 67, 866–897. https://doi.org/10.1175/2009JAS2995.1.
Oltmans, S.J., Lefohn, A.S., Harris, J.M., Shadwick, D.S., 2008. Background ozone levels of air entering the west coast of the US and assessment of longer-term changes. Atmos. Environ. 42, 6020–6038. https://doi.org/10.1016/j.atmosenv.2008.03.034. https://search.crossref.org/?q=Oltmans%2C+S.+J.%2C+Lefohn%2C+A.+S.%2C+Harris%2C+J.+M.%2C+and+Shadwick%2C+D.+S.+%282008%29%2C+Background+ozone+levels+of+air+entering+the+west+coast+of+the+US+and+assessment+of+longer-term+changes.+Atmos.+Environ.%2C+42%2C+6020-6038.
Ostro, B.D., Tran, H., Levy, J.I., 2012. Health benefits of reduced tropospheric ozone in California. J. Air Waste Manag. Assoc. 56, 1007–1021. https://doi.org/10.1080/10473289.2006.10464511.

Parrish, D.D., Aikin, K.C., Oltmans, S.J., Johnson, B.J., Ives, M., Sweeny, C., 2010. Impact of transported background ozone inflow on summertime air quality in a California ozone exceedance area. Atmos. Chem. Phys. 10, 10093–10109. https://doi.org/10.5194/acp-10-10093-2010.

Parrish, D.D., et al., 2014. Long-term changes in lower tropospheric baseline ozone concentrations: comparing chemistry-climate models and observations at northern midlatitudes. J. Geophys. Res. Atmos. 119, 5719–5736. https://doi.org/10.1002/2013JDo21435.

Parrish, D.D., Petropavlovskikh, I., Oltmans, S.J., 2017. Reversal of long-term trend in baseline ozone concentrations at the north American west coast. Geophys. Res. Lett. 44, 10675–10681. https://doi.org/10.1002/2017GL074960.

Pfister, G.G., Wiedinmyer, C., Emmons, L.K., 2008. Impacts of the fall 2007 California wildfires on surface ozone: integrating local observations with global model simulations. Atmos. Sci. 35, L19814. https://doi.org/10.1029/2008GL034747.

Pudasainee, D., Sapkota, B., Shrestha, M.L., Kaga, A., Kondo, A., Inoue, Y., 2006. Ground level ozone concentrations and its association with NOx and meteorological parameters in Kathmandu valley, Nepal. Atmos. Environ. 40, 8081–8087. https://doi.org/10.1016/j.atmosenv.2006.07.011.

Pusede, S.E., Cohen, R.C., 2012. On the observed response of ozone to NO_x and VOC reactivity reductions in San Joaquin Valley California 1995-present. Atmos. Chem. Phys. 12, 8323–8339. https://doi.org/10.5194/acp-12-8323-2012.

Rai, R., Agrawai, M., 2012. Impact of tropospheric ozone on crop plants. Proc. Natl. Acad. Sci. India B Biol. Sci. 82, 241–257. https://doi.org/10.1007/s40011-012-0032-2.

Rasmussen, D.J., Fiore, A.M., Naik, V., Horowitz, L.W., McGinnis, S.J., Schultz, M.G., 2012. Surface ozone-temperature relationships in the eastern US: a monthly climatology for evaluating chemistry-climate models. Atmos. Environ. 47, 142–153. https://doi.org/10.1016/j.atmosenv.2011.11.021 (2012) 142e153. https://search.crossref.org/?q=Rasmussen%2C+D.+J.%2C+Fiore%2C+A.+M.%2C+Naik%2C+V.%2C+Horowitz%2C+L.W.%2C+McGinnis%2C+S.+J.%2C+and+Schultz%2C+M.+G.+%282012%29%2C+Surface+ozone-temperature+relationships+in+the+eastern+US%3A+a+monthly+climatology+for+evaluating+chemistry-climate+models.+Atmos.+Environ.%2C+47%2C+142-153.

Ryoo, J., Johnson, M.S., Iraci, L.T., Yates, E.L., Gore, W., 2017. Investigating sources of ozone over California using AJAX airborne measurements and models: assessing the contribution from long-range transport. Atmos. Environ. 155, 53–67. https://doi.org/10.1016/j.atmosenv.2017.02.008.

Seaman, N.L., Michelson, S.A., 2000. Mesoscale meteorological structure of a high-ozone episode during the 1995 NARSTO-northeast study. J. Appl. Meteorol. 39, 384–398. https://doi.org/10.1175/1520-0450(2000)039<0384:MMSOAH>2.0.CO;2.

Seidel, D.J., Ao, C.O., Li, K., 2010. Estimating climatological planetary boundary layer heights from radiosonde observations: comparison of methods and uncertainty analysis. J. Geophys. Res. 115 https://doi.org/10.1029/2009JD013680.

Shindell, D.W., Faluvegi, G., Bell, N., Schmidt, G.A., 2005. An emissions-based view of climate forcing by methane and tropospheric ozone. Geophys. Res. Lett. 32 https://doi.org/10.1029/2004GL021900.

Simon, H., Reff, A., Wells, B., Xing, J., Frank, N., 2015. Ozone trends across the United States over a period of decreasing NOx and VOC emissions. Eviron. Sci. Technol. 49, 186–195. https://doi.org/10.1021/es504514z.

Smit, H.G.J., Straeter, W., Johnson, B.J., Oltmans, S.J., Davies, J., Tarasick, D.W., Hoegger, B., Stubi, R., Schmidlin, F.J., Northam, T., Thompson, A.M., Witte, J.C., Boyd, I., Posny, F., 2007. Assessment of the performance of ECC-ozonesondes under quasi-flight conditions in the environmental simulation chamber: insights from the Juelich ozone sonde intercomparison experiment (JOSIE). J. Geophys. Res. 112 https://doi.org/10.1029/2006JD007308.

Smith, K.R., et al., 2009. Public health benefits of strategies to reduce greenhouse-gas emissions: health implications of short-lived greenhouse pollutants. Lancet 374 (9707), 2035–2038. https://doi.org/10.1016/S0140-6736(09)61716-5.

Sprenger, M., Wernli, H., Bourqui, M., 2007. Stratosphere-troposphere exchange and its relation to potential vorticity streamers and cutoffs near the extratropical tropopause. J. Atmos. Sci. 64, 1587–1602. https://doi.org/10.1175/JAS3911.1.

Task Force on Hemispheric Transport of Air Pollution, 2010. Hemispheric Transport of Air Pollution 2010 Part A: Ozone and Particulate Matter available at. http://pure.iiasa.ac.at/id/eprint/14571/1/HTAP%202010%20Part%20A%20110407.pdf.

Tu, J., Xia, Z., Wang, H., Li, W., 2007. Temporal variations in surface ozone and its precursors and meteorological effects at an urban site in China. Atmos. Res. 85, 310–337. https://doi.org/10.1016/j.atmosres.2007.02.003.

Turner, M.C., et al., 2016. Long-Term ozone exposure and mortality in a large prospective study. Am. J. Respir. Crit. Care Med. 193, 1134–1142. https://doi.org/10.1164/rccm.201508-1633OC.

U.S. Environmental Protection Agency, 1998. National Air Quality and Emissions Trends Report, 1997, available at. https://www.epa.gov/sites/production/files/2017-11/documents/trends_report_1997.pdf.

Wang, X.Y., Wang, K.C., 2014. Estimation of atmospheric mixing layer height from radiosonde data. Atmos. Meas. Tech. 7, 1701–1709. https://doi.org/10.5194/amt-7-1701-2014.

Wei, W., Cheng, S., Li, G., Wang, G., Wang, H., 2014. Characteristics of ozone and ozone precursors (VOCs and NO_x) around a petroleum refinery in Beijing, China. J. Environ. Sci. 26, 332–342. https://doi.org/10.1016/S1001-0742(13)60412-X.

West, J.J., Fiore, A.M., Horowitz, L.W., Mauzerall, D.L., 2006. Global health benefits of mitigating ozone pollution with methane emission controls. Proc. Natl. Acad. Sci. Unit. States Am. 103, 3988–3993. https://doi.org/10.1073/pnas.0600201103.

Wigder, N.L., Jaffe, D.A., Herron-Thorpe, F.L., Vaughan, J.K., 2013. Influence of daily variations in baseline ozone on urban air quality in the United States Pacific Northwest. J. Geophys. Res. Atmos. 118, 3343–3354. https://doi.org/10.1029/2012/JD018738.

Wu, S., Mickley, L.J., Jacob, D.J., Rind, D., Streets, D.G., 2008. Effects of 2000-2050 changes in climate and emissions on global tropospheric ozone and the policy-relevant background surface ozone in the United States. J. Geophys. Res. 113 https://doi.org/10.1029/2007JD009639.

Xiao, X., Cohan, D.S., Byun, D.W., Ngan, F., 2010. Highly nonlinear ozone formation in the Houston region and implications for emission controls. J. Geophys. Res.: Atmos. 115 https://doi.org/10.1029/2010JD014435.

Yates, E.L., Iraci, L.T., Roby, M.C., Pierce, R.B., Johnson, M.S., Reddy, P.J., Tadić, J.M., Loewenstein, M., Gore, W., 2013. Airborne observations and modeling os springtime stratosphere-to-troposphere transport over California. Atmos. Chem. Phys. 13, 12481–12494. https://doi.org/10.5194/acp-13-12481-2013.

Zhang, L., Jacob, D.J., Yue, X., Downey, N.V., Wood, D.A., Blewitt, D., 2014. Sources contributing to background surface ozone in the US Intermountain West. Atmos. Chem. Phys. 14, 5295–5309. https://doi.org/10.5194/acp-14-5295-2014.